IEEE Transactions on Automation Science and Engineering (T-ASE) paper, presented at ICRA 2024, Yokohama, Japan.
Cite as T-ASE paper.

Semi-analytical Design of PDE Endpoint Controller for Flexible Manipulator with Non-homogenous Boundary Conditions

S. Yaqubi, S. M. Tahamipour-Z., and J. Mattila

***Abstract*—This study proposes a new semi-analytical design and implementation method for nonlinear partial differential equation (PDE) control of a flexible manipulator. The proposed scheme considers the effects of the boundary input force and gravity on the payload, which results in non-homogenous boundary conditions. This objective is achieved based on a model transformation scheme for homogenizing boundary conditions, obtaining semi-analytical solutions for the corresponding PDE model. Model transformation is assigned as a hybrid exponential–polynomial function whose coefficients are conveniently calculable without the need for any additional boundary condition measurements. This eliminates the need to use intensive numerical solvers—for example, methods based on finite element analysis—and allows the implementation of sophisticated PDE control schemes considering fully nonlinear PDE models with high computation speed. The presented controller is robust to parametric model uncertainty due to its adaptive design. The precision and efficiency of calculating distributed states using the proposed model transformation are demonstrated based on experimental data for the flexible manipulator with respect to the ground truth camera-based motion capture system. Model transformation is also numerically implemented for the proposed nonlinear endpoint control method based on the original PDE model. Note to practitioners—This paper investigates the difficulty of obtaining data describing the flexible manipulator pose required for precise control and analysis and proposes a computationally efficient method to overcome this issue.**

***Index Terms*—PDE control; flexible manipulator; non-homogenous boundary conditions; endpoint control; distributed state estimation.**

I. INTRODUCTION

THE INCREASING APPLICATION of flexible structures has been a significant trend in modern industry due to their capacity for achieving higher efficiency and reduced weight. Correspondingly, they have attracted significant research attention with respect to their design, analysis, and, more recently, control. Achieving the true potential of flexible systems is not possible without considering the properties that make them unique in the first place. Flexible structures are described by dynamic models that differ significantly from their rigid counterparts. They are distinctly continuous systems in which each element must be considered within a larger framework for mathematically precise modeling and motion analysis purposes. This objective is attainable by describing flexible system dynamics using appropriate partial differential equation (PDE) models. There are various methods through which PDE models for flexible systems can be obtained. This includes linearized models for multibody flexible systems [1] and nonlinear models for flexible robotics [2] using standard flexible structure modeling theories—for example, Euler–Bernoulli and Timoshenko beam theory [3]. However, the application of flexible system models for control purposes has proven to be challenging, hindering their application in autonomous robotics.

For precise control and motion-planning tasks, even standard applications, such as endpoint control of a robot with a payload, may require thorough analysis of nonlinear PDEs where standard principles, such as separation-of-variables, are not readily applicable. Hence, simplified models and various reductions are often applied for the implementation of control techniques. Such simplifications may be in the form of PDE model approximations such as ordinary differential equations (ODE) [4], finite element methods [5], or physical approximations such as modeling link flexibility as lumped springs [6]. The interest in more sophisticated techniques has inspired recent research works that implement PDE models directly in control calculations to obtain more precise control actions [2], [7]–[11]. Various modifications of this approach have allowed the consideration of different effects including mitigation of endpoint deflection through the exertion of control action on boundary conditions of the mechanism [12], input nonlinearity and backlash effects [13], and control of flexible manipulators in three-dimensional space [14]. Recently, researchers have evaluated problems corresponding to modeling uncertainty in flexible structures. Model uncertainty is inevitable in many flexible systems due to the intricate modeling procedures required in such systems and the multitude of physical, geometric, and mechanical properties in effect [15]. Research on this topic includes adaptive control of manipulators with unknown control directions [16], cooperative control of dual-flexible manipulators [17], and neural network-based controllers for adaptive control of flexible structures [18].

Advancements have been achieved in the flexible system

This work was supported by the Academy of Finland under the project "High precision autonomous mobile manipulators for future digitalized construction site" [Grant No. 335569]. (Corresponding author: S. Yaqubi)

S. Yaqubi, S. M. Tahamipour-Z., and J. Mattila are with the Department of Automation Technology and Mechanical Engineering, Tampere University, Korkeakoulunkatu 6, 33720 Tampere, Finland (e-mails: sadeq.yaqubi@tuni.fi, seyedmohammad.tahamipourzarandi@tuni.fi, and jouni.mattilia@tuni.fi).

control field in recent years, but there are still topics that have been relatively unexplored. Among them is the issue of the intensiveness of PDE calculations. In many PDE control strategies, the mathematical model is not conveniently solvable due to the existence of various nonlinearities and non-homogenous boundary conditions. Non-homogenous boundary conditions are not strictly functions of distributed states and their higher-order derivatives. Therefore, they do not allow for precise calculation of spatial functions describing the mode shapes of the structure, as they are not readily solvable using separation of variables [19]. This is also the case for many boundary control strategies, as the control input itself is usually defined based on the error signal [2], [20] and is not a function of the distributed states themselves. Thus, exerting input in boundary locations may also render the system non-homogenous. As a result, while the control structure may be designed based on rigorous mathematical analysis, appropriate tools are not necessarily available for application in an analytical or semi-analytical manner. Analytic or semi-analytic PDE solutions have often been investigated for lower-order PDEs—for example, a heat transfer problem in an open-loop framework [21]. However, this approach is challenging for higher-order beam PDEs, especially for closed-loop systems. This has led to the use of numerical methods, such as finite-element analysis (FEA), for the implementation of PDE-based control methods [2], [22], [23].

The issue of a lack of information on distributed states describing the configuration of a flexible link—that is, the displacement of elements of a link and their higher-order derivatives—is significant. Studies that solely focus on the control of flexible manipulators often forgo this aspect under the assumption that the displacement of a flexible link and its higher-order derivatives is measurable [24]. However, this is often not the case. In practice, only a limited number of measurement samples are considered, even though flexible link dynamics are continuous and have infinite dimensions. As a result, the generated map for the displacement of the flexible link is potentially inaccurate in samples that are not directly located on measurement points. This inaccuracy is even more notable for higher-order derivatives of displacement terms [25], which can be obtained using numerical differentiation when analytical displacement mapping is not available. Hence, information describing the dynamics of flexible links throughout the length cannot be readily implemented. This leads to the incalculability of dynamic terms featuring distributed states throughout the link [26]. In such cases, a feasible input may depend only on boundary information, which limits control over the distributed states themselves. Recent research studies have proposed various observation and estimation schemes that have been able to recover distributed information based on limited boundary measurements. However, introducing additional observation and estimation dynamics also affects the intensiveness of numerical calculations. Furthermore, existing state estimation schemes have been obtained in cases without input dependency [23], [27], [28] or those introducing additional subsystems [29], which may affect computational intensity, as this results in an increase in the number of equations required to describe system dynamics.

It has been discussed that the combination of intensive PDE-based calculations, the need for recovery of missing distributed state information, and the high calculation burden of obtaining numerical solutions for involved PDEs potentially renders the implementation of such control schemes unfeasible. Furthermore, standard numerical solvers are often incapable of providing precise information for control calculations corresponding to distributed states, and their calculations require further numerical manipulation.

In this work, we address the aforementioned issues by presenting a mathematical scheme for model transformation in the dynamic applications of flexible manipulators. This leads to a PDE model with homogenous boundary conditions that can be readily used for the construction of sophisticated PDE control strategies and enables semi-analytical solutions for calculating control input. A nonlinear controller is presented for endpoint tracking and the elimination of undesired deflections, which are implemented using the aforementioned model transformation scheme. In brief, the novel contributions of this work are expressed as follows: (i) a novel model transformation scheme is presented for homogenizing the Euler–Bernoulli PDE flexible manipulator model with non-homogenous boundary conditions, boundary input, and payload gravity effects; (ii) a new nonlinear adaptive PDE controller is presented for endpoint and state tracking as well as elimination of undesired deflections; (iii) the procedure for obtaining a semi-analytical solution for a closed-loop system is detailed, enabling implementation of control calculations and estimation of flexible link distributed states with high calculation speed; and (iv) the precision and efficiency of the model transformation scheme is verified for a flexible manipulator using a ground truth camera-based motion capture system.

The rest of this paper is organized as follows. Section II presents a general Euler–Bernoulli model for flexible manipulators with boundary input as well as problem preliminaries. Section III features the construction of a nonlinear PDE-based control model. Section IV details the model transformation procedure. A discussion regarding the implementation and solvability of the model is presented in Section V. The effectiveness and efficiency of the procedure are investigated in Section VI through numerical and experimental analysis.

II. Problem Statement and Preliminaries

The primary objective of this work is to obtain an appropriate model transformation procedure for dynamic flexible structures. To address this issue, the case of a one-link flexible manipulator with gravity effects and payload is investigated [30]–[33]. The mechanism consists of a flexible link in the vertical plane and is depicted in Fig. 1. In this study, the flexible arm is modeled as an infinite-dimensional beam with distributed displacement states $\omega(\xi)$, where ξ indicates the position of a flexible beam element alongside its longitudinal axis; t is the system time; l, A, ρ, E, and I indicate the length,

cross-section area, mass density, elastic modulus, and surface moment of beam inertia, respectively. θ expresses the angle of the beam with respect to a designated $O(x,y)$ coordinate system. Lumped mass M is installed at the end of the flexible beam and acts as the payload of the mechanism. Input torque τ is exerted to joint O, and boundary input force u acts on the endpoint of a beam located at $\xi = l$. In practice, input torque may be generated by rotary actuators—for example, DC electric gear motors. The boundary input force is applicable through force actuators, such as hydraulic or pneumatic actuators. Input torque is also applicable through an equivalent force using force actuators exerted at a predetermined distance from the joint.

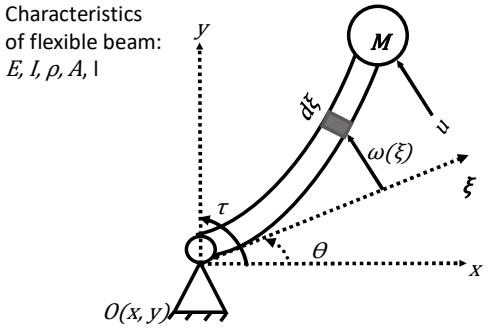

Fig. 1. Schematic of a one-link flexible manipulator with a payload.

The extended Hamilton principle [3] is used in this study to obtain the mathematical model for the described dynamic system considering planar motion and transverse displacement of a flexible link.

Assumption 1. It is assumed that the flexible link does not feature longitudinal displacement effects.

To obtain the flexible system model featuring distributed states, the position vector $\bar{\boldsymbol{r}}_\xi$ for an infinitesimal element of a flexible beam located at coordinate ξ with respect to the connecting joint and position vector for the $\bar{\boldsymbol{r}}_M$ of the payload are expressed as in (1)–(4).

$$\bar{\boldsymbol{r}}_\xi = \begin{bmatrix} r_{x,\xi} \\ r_{y,\xi} \end{bmatrix} \tag{1}$$

$$r_{x,\xi} = \xi\cos\theta - \omega(\xi)\sin\theta \tag{2}$$

$$r_{y,\xi} = \xi\sin\theta + \omega(\xi)\cos\theta \tag{3}$$

$$\bar{\boldsymbol{r}}_M = \bar{\boldsymbol{r}}_l \tag{4}$$

According to the Euler–Bernoulli beam theory, the kinetic energy T resulting from the motion of the flexible link elements and endpoint mass, potential energy V based on deformation of the flexible link elements and gravity effects, and generalized force corresponding to the entire mechanism are described as follows:

$$T = \frac{1}{2}\rho A\int_0^l \dot{\bar{\boldsymbol{r}}}_\xi^T\dot{\bar{\boldsymbol{r}}}_\xi\, d\xi + M\dot{\bar{\boldsymbol{r}}}_l^T\dot{\bar{\boldsymbol{r}}}_l, \tag{5}$$

$$V = \frac{1}{2}mgl\sin\theta + Mgl\sin\theta + Mg\omega(l)\cos\theta + \frac{1}{2}\int_0^l\left[\frac{\partial^2\omega(\xi)}{\partial\xi^2}\right]^2 d\xi, \tag{6}$$

$$\delta W = \tau\delta\theta + \underline{\boldsymbol{u}}_l^T\delta\bar{\boldsymbol{r}}_l. \tag{7}$$

The notation $[\dot{-}]$ expresses the derivative of the bracketed term with respect to time. The boundary input vector expressed in $O(x,y)$ is as follows: $\underline{\boldsymbol{u}}_l = \left[u\cos(\frac{\pi}{2}+\theta), u\sin(\frac{\pi}{2}+\theta)\right]^T$. Substituting (5)–(7) in the extended Hamilton principle $\delta(T - V + W) = 0$ and based on the calculation of variation terms listed in Appendix A, a mathematical model for system dynamics featuring governing equations and boundary conditions is obtained as (8)–(12).

$$\begin{aligned}[I_m + Ml^2 + M\omega^2(l)]\ddot{\theta} + Ml\omega_{tt}(l) + 2M\omega(l)\omega_t(l) \\ + \rho A\int_0^l\left[2\omega(\xi)\omega_t(\xi)\dot{\theta} + \omega^2(\xi)\ddot{\theta}\right. \\ \left. + \xi\omega_{tt}(\xi)\right]d\xi + \frac{1}{2}mgl\cos\theta \\ + Mgl\cos\theta + Mg\omega(l)\sin\theta = \tau + ul\end{aligned} \tag{8}$$

$$\omega_{tt}(\xi) - \omega(\xi)\dot{\theta}^2 + \xi\ddot{\theta} + \frac{EI}{\rho A}\omega_{\xi\xi\xi\xi}(\xi) = 0 \tag{9}$$

$$\omega_{tt}(l) - \omega(l)\dot{\theta}^2 + l\ddot{\theta} + g\cos\theta - \frac{EI}{M}\omega_{\xi\xi\xi}(l) = u \tag{10}$$

$$\omega(0) = \omega_\xi(0) = 0 \tag{11}$$

$$\omega_{\xi\xi}(l) = 0 \tag{12}$$

where $m = \rho Al$ is the mass of the flexible beam. The mass moment of inertia of a rigid beam with identical density and geometric properties is expressed as $I_m = \frac{1}{3}\rho Al^3$. For brevity, expressions $\omega_\xi = \frac{\partial\omega}{\partial\xi}$ and $\omega_t = \frac{\partial\omega}{\partial t}$ are used to indicate partial derivatives of distributed states.

Remark 1. Boundary condition (10) is not strictly a function of distributed state $\omega(\xi)$ and its higher-order derivatives $\frac{\partial\omega^n(\xi)}{\partial\xi^n}$ and $\frac{\partial\omega^m(\xi)}{\partial t^m}$ (where m and n attain positive integer values), as input term u and gravity term $g\cos\theta$ do not strictly correspond to distributed states. Hence, model (8)–(12) features non-homogenous boundary conditions.

Remark 2. The solution of nonlinear PDE model (8)–(12), featuring non-homogenous boundary conditions, cannot be readily obtained using analytical methods since standard principles, such as separation-of-variables, are not applicable. Furthermore, semi-analytical methods utilizing basis orthogonal functions would be difficult to implement, as the orthogonal basis—that is, mode shapes in assumed mode methods (as described in detail in Section V)—is not obtainable, given non-homogenous boundary conditions (10). Hence, FEA models and other numerical solvers have often been employed for corresponding controllers [2], [22], [34].

Based on Remark 1, further developments are needed to enable the implementation of a control model based on nonlinear PDEs with high calculation speed using semi-analytical methods. To address this issue, we propose a strategy based on the design of a PDE controller for a flexible manipulator (in Section III), obtaining an appropriate model transformation for homogenizing a flexible manipulator model (in Section IV), and calculating distributed state values using the aforementioned model transformation (in Section V).

III. Boundary Control of Flexible Systems

This section details the construction of a nonlinear boundary controller for state tracking and the elimination of undesired deflections throughout the length of a flexible link, as well as endpoint displacement.

Remark 3. The primary control objectives are the tracking of the reference joint angle signal θ_r and the elimination of endpoint displacement $\omega(l)$, which results in tracking of the corresponding endpoint trajectory (x_r, y_r). Elimination of undesired deflection throughout the length of the flexible beam $\omega(\xi)$ for $\xi \in (0, l)$ is considered the secondary control objective. The closed-loop system features two input signals—that is, joint torque τ and boundary input u—as well as outputs θ and $\omega(\xi), \xi \in [0, l]$. It is desirable that the controller be assigned such that it enables the convenient investigation of interactions between multiple inputs and outputs in a MIMO framework.

To eliminate the integral term $\int_0^l \xi \omega_{tt}(\xi) d\xi$ governing equations of motion, (8)–(12) are rewritten as (13). Initially, (9) is multiplied in ξ and then integrated over the length of the flexible beam.

$$\int_0^l \xi \omega_{tt}(\xi) d\xi = \dot{\theta}^2 \int_0^l \xi \omega(\xi) d\xi - \frac{EI}{\rho A} \int_0^l \xi \omega_{\xi\xi\xi\xi}(\xi) d\xi - \frac{1}{3} l^3 \ddot{\theta}. \tag{13}$$

Substituting (13) in (8), it follows that:

$$\begin{aligned} &\left[I + Ml^2 + M\omega^2(l) + \rho A \int_0^l \omega^2(\xi)\, d\xi - \frac{1}{3}\rho A l^3\right] \ddot{\theta} + \\ &Ml\omega_{tt}(l) + 2M\omega(l)\omega_t(l) + 2\rho A \int_0^l \omega(\xi)\omega_t(\xi)\dot{\theta}\, d\xi + \\ &\frac{1}{2} mgl \cos\theta + Mgl\cos\theta + Mg\omega(l)\sin\theta + \\ &\dot{\theta}^2 \int_0^l \xi\omega(\xi) d\xi - \frac{EI}{\rho A} \int_0^l \xi \omega_{\xi\xi\xi\xi}(\xi) d\xi = \tau + ul. \end{aligned} \tag{14}$$

As expressed in Remark 3, (10) and (14) are used to construct the controller for the objective of endpoint trajectory tracking, and (9) is incorporated into the control calculation such that $\omega(\xi)$ is bounded and decays to zero.

For convenience, (10) and (14) are expressed in matrix form.

$$\underline{\boldsymbol{M}}\, \underline{\ddot{\boldsymbol{q}}} + \underline{\boldsymbol{h}} = \underline{\boldsymbol{B}}\, \underline{\boldsymbol{u}} \tag{15}$$

$$\underline{\boldsymbol{M}} = \begin{bmatrix} I + Ml^2 + M\omega^2(l) + \rho A \int_0^l \omega^2(\xi)\, d\xi - \frac{1}{3}\rho A l^3, & Ml \\ 1, & l \end{bmatrix} \tag{16}$$

$$\underline{\boldsymbol{q}} = \begin{bmatrix} \theta \\ \omega(l) \end{bmatrix} \tag{17}$$

$$\underline{\boldsymbol{h}} = \begin{bmatrix} \underline{\boldsymbol{h}}_1 \\ \underline{\boldsymbol{h}}_2 \end{bmatrix} \tag{18}$$

$$\begin{aligned} \underline{\boldsymbol{h}}_1 = {} & 2M\omega(l)\omega_t(l) + 2\rho A \int_0^l \omega(\xi)\omega_t(\xi)\dot{\theta}\, d\xi \\ & + \frac{1}{2} mgl\cos\theta + Mgl\cos\theta \\ & + Mg\omega(l)\sin\theta + \dot{\theta}^2 \int_0^l \xi\omega(\xi) d\xi \\ & - \frac{EI}{\rho A} \int_0^l \xi \omega_{\xi\xi\xi\xi}(\xi) d\xi \end{aligned} \tag{19}$$

$$\underline{\boldsymbol{h}}_2 = -\omega(l)\dot{\theta}^2 + g\cos\theta - \frac{EI}{M}\omega_{\xi\xi\xi}(l) \tag{20}$$

$$\underline{\boldsymbol{B}} = \begin{bmatrix} 1, & l \\ 0, & 1 \end{bmatrix} \tag{21}$$

$$\underline{\boldsymbol{u}} = \begin{bmatrix} \tau \\ u \end{bmatrix} \tag{22}$$

Given the control objectives expressed in Remark 3, the error dynamics of the controller are defined as follows:

$$\underline{\dot{\boldsymbol{e}}} = \underline{\boldsymbol{\nu}} + \underline{\boldsymbol{\gamma}}\, \underline{\boldsymbol{u}}, \tag{23}$$

$$\underline{\boldsymbol{e}} = \begin{bmatrix} \dot{\theta} - \dot{\theta}_r + \lambda_\theta(\theta - \theta_r) \\ \dot{\omega}(l) + \lambda_\omega \omega(l) \end{bmatrix}, \tag{24}$$

$$\underline{\boldsymbol{\nu}} = -\underline{\boldsymbol{M}}^{-1} \underline{\boldsymbol{h}} + \begin{bmatrix} -\ddot{\theta}_r + \lambda_\theta(\dot{\theta} - \dot{\theta}_r) \\ \lambda_\omega \omega_t(l) \end{bmatrix}, \tag{25}$$

$$\underline{\boldsymbol{\gamma}} = \underline{\boldsymbol{M}}^{-1} \underline{\boldsymbol{B}}, \tag{26}$$

where $|\lambda_\theta| > 1$ and $|\lambda_\omega| > 1$ are control parameters. When obtaining the control law, we address individual elements of (23) as $\underline{\boldsymbol{e}} = [e_1, e_2]^T$.

$$\dot{e}_1 = \nu_1 + \gamma_{11} u_1 + \gamma_{12} u_2 \tag{27}$$

$$\dot{e}_2 = \nu_2 + \gamma_{21} u_1 + \gamma_{22} u_2 \tag{28}$$

To compensate for the effects of potential parametric uncertainty, control action is designed such that it features parametric adaptation. To this end, the system parameter vector is defined as follows:

$$\underline{\boldsymbol{s}} = [M, \quad s_2, \quad l, \quad m]^T, \tag{29}$$

where $s_2 = \frac{EI}{\rho A}$. The estimated parameter vector $\underline{\hat{\boldsymbol{s}}}$ is used in the construction of the control scheme. Additionally, it is assumed that $\underline{\boldsymbol{s}}$ is bounded according to Assumption 1.

Assumption 2. It is considered that the lower and upper bounds for $\underline{\boldsymbol{s}}$ are known as $\underline{\boldsymbol{s}}_l < \underline{\boldsymbol{s}} < \underline{\boldsymbol{s}}_h$. This is expressed as $\underline{\boldsymbol{s}} \in \mathcal{Q}$, where $\mathcal{Q}$ indicates the defined uncertainty space.

Based on the definition of $\underline{\boldsymbol{s}}$, all elements of $\underline{\boldsymbol{s}}_l$ and $\underline{\boldsymbol{s}}_h$ attain strictly positive values. The parametric estimation error is defined as follows:

$$\underline{\tilde{\boldsymbol{s}}} = \underline{\boldsymbol{s}} - \underline{\hat{\boldsymbol{s}}}. \tag{30}$$

On this basis, a projection function with respect to uncertainty space $\mathcal{Q}$ is assignable for given values s, s_l, s_h, and e, where s_l and s_h indicate lower and upper uncertainty bounds for s.

$$\mathcal{P}(s, s_l, s_h, e) = \begin{cases} 0, if\ \mathcal{P} \geq\ s_h\ and\ e > 0 \\ 0, if\ \mathcal{P} \leq\ s_l\ and\ e < 0 \\ e, otherwise \end{cases} \tag{31}$$

Lemma 1. If $\dot{\hat{s}} = \mathcal{P}(\hat{s}, s_l, s_h, e)$ is assigned, the following holds:

$$s_l < \hat{s} < s_h, \tag{32}$$

$$(s - \hat{s})[e - \mathcal{P}(\hat{s}, s_l, s_h, e)] \leq 0. \tag{33}$$

Proof. The proof is a standard property of projection functions [26] and is omitted.

Theorem 1. Control law (34) and parameter adaptation law (35) ensure the satisfaction of control objectives expressed in Remark 3 and the asymptotic stability of the closed-loop system.

$$\underline{\hat{\boldsymbol{u}}} = \widehat{\boldsymbol{\mathcal{M}}}^{-1} \widehat{\boldsymbol{\hbar}} \tag{34}$$

$$\underline{\dot{\hat{\boldsymbol{s}}}} = \mathcal{P}(\underline{\boldsymbol{s}}, \underline{\boldsymbol{s}}_l, \underline{\boldsymbol{s}}_h, \underline{\boldsymbol{\lambda}}_{\mathcal{Q}} + \underline{\boldsymbol{\Lambda}}_{\mathrm{s}}) \tag{35}$$

$\widehat{\boldsymbol{\mathcal{M}}}$, $\widehat{\boldsymbol{\hbar}}$, and $\underline{\boldsymbol{\Lambda}}_{\mathrm{s}}$ are functions of the system dynamics, corresponding Lyapunov function, and reference signals, respectively. $\underline{\boldsymbol{\lambda}}_{\mathcal{Q}}$ is assigned with respect to uncertainty space $\mathcal{Q}$. Exact expressions are listed in the proof.

Proof. The proof is detailed in Appendix B.

Remark 4. In the proof of Theorem 1, Cauchy–Schwartz inequality and a modified form of Nash inequality [35] proposed by Rahn [36] (see Lemma 12) are used, indicating that

$\int_0^l \omega_\xi^2\, d\xi \geq \frac{1}{l^2}\int_0^l \omega_{\xi\xi}\, d\xi$, given the satisfaction of conditions compatible with the system investigated in this work.

Remark 5. Obtaining control input and parameter update rule (34) and (35) requires calculation of integrated terms featuring the distributed states. The integrated terms are in the form of $\int_0^l f\left[\omega(\xi), \omega_t(\xi), \omega_\xi(\xi), \omega_{\xi\xi\xi\xi}(\xi)\right] d\xi$. Hence, with respect to both ξ and t, displacement mapping $\omega(\xi)$ should be continuous and differentiable. In practice, obtaining displacement values for the length of a flexible beam using direct distributed measurements is often not feasible as it requires sensor installation for all samples in the flexible link. On this basis, practical displacement mapping using solely the information obtained at boundary points $\xi = 0$ and $\xi = l$ should be attained. This objective is accomplished using the estimation model proposed in Section IV.

IV. Model Transformation for Homogenizing Boundary Conditions

In this section, a model transformation for (8)–(12) is derived such that the corresponding boundary conditions are homogenized. This obtains a semi-analytical solution for the PDE model of closed-loop systems and provides continuous differentiable mapping for the displacement of a flexible link.

To obtain a model transformation function satisfying the properties of the investigated manipulator, it is set that $\xi = l$ in (9), and the resulting equation is substituted in (10) to eliminate higher-order temporal derivatives and obtain modified boundary conditions (36).

$$\omega_{\xi\xi\xi\xi}(l) + \frac{\rho A}{M}\omega_{\xi\xi\xi}(l) = -\kappa u + \kappa g \cos\theta, \tag{36}$$

where $\kappa = \frac{\rho A}{EI}$. For the rest of this paper, (36) is used instead of (10) for boundary conditions. The modified model (8), (9), (11), (12), and (36) is investigated for homogenizing boundary conditions. On this basis, we propose the following model transformation, featuring homogenized boundary conditions for variable $z(\xi)$:

$$z(\xi) = \omega(\xi) + \nu(\xi), \tag{37}$$

$$z(0) = z_\xi(0) = 0, \tag{38}$$

$$z_{\xi\xi}(l) = 0, \tag{39}$$

$$z_{\xi\xi\xi\xi}(l) + \frac{\rho A}{M} z_{\xi\xi\xi}(l) = 0. \tag{40}$$

$\nu(\xi)$ has to be determined such that it satisfies conditions (41)–(45):

$$\nu(0) = \nu_\xi(0) = 0, \tag{41}$$

$$\nu(l) = \nu_{\xi\xi}(l) = 0, \tag{42}$$

$$\nu_{\xi\xi\xi\xi}(l) + p\nu_{\xi\xi\xi}(l) = f_b^*, \tag{43}$$

$$f_b^* = \kappa u - \kappa g \cos\theta, \tag{44}$$

$$p = \frac{\rho A}{M}. \tag{45}$$

Model transformation variable (46) is proposed based on (43).

$$\begin{aligned}\nu(\xi) &= \int_0^\xi \int_0^\xi \int_0^\xi \left(\frac{c}{p}e^{-p\xi} + \frac{f_b^*}{p}\right) d\xi \\ &= -\frac{c_e}{p^4}e^{-p} + \frac{1}{6}\frac{f_b^*}{p}\xi^3 + c_2\xi^2 + c_1\xi \\ &\quad + c_0\end{aligned} \tag{46}$$

Coefficients c_0, c_1, c_2, and c_e are calculated such that they satisfy (41) and (42).

$$c_0 = \frac{c}{p^4} \tag{47}$$

$$c_1 = -\frac{c}{p^3} \tag{48}$$

$$c_2 = \frac{c}{2p^2}e^{-pl} - \frac{l}{2p}f_b^* \tag{49}$$

$$c = \gamma_1 f_b^* \tag{50}$$

$$\gamma_1 = \frac{2p^3 l^3}{(3p^2l^2 - 6)e^{-pl} + 6 - 6pl} \tag{51}$$

Substituting (47)–(51) in (46), $\nu(\xi)$ is calculated as follows:

$$\nu(\xi) = \gamma(\xi) f_b^*, \tag{52}$$

$$\gamma(\xi) = -\frac{\gamma_1}{p^4}e^{-p\xi} + \frac{1}{6p}\xi^3 + \gamma_2\xi^2 - \frac{\gamma_1}{p^3}\xi + \frac{\gamma_1}{p^4}, \tag{53}$$

where $\gamma_2 = \frac{\gamma_1}{2p^2}e^{-pl} - \frac{l}{2p}$.

Remark 6. The boundary conditions for $\nu(\xi)$ are functions of the higher-order derivative $\omega_{\xi\xi\xi\xi}(l)$. To satisfy these conditions using standard polynomial solutions, measurements of up to the fourth-order derivative of the endpoint deflection are needed for homogenizing original boundary conditions. However, using the proposed hybrid polynomial–exponential function (46), exerting only one additional condition $\nu(l) = 0$ is sufficient for obtaining all required coefficients.

Remark 7. In this paper, model transformation term (52) is obtained for boundary control of a flexible manipulator, following boundary conditions (10)–(12). For different classes of flexible manipulators, corresponding model transformation terms are calculable by substituting dynamic equations or equations describing the displacement of a flexible link (equivalent to (9)) for endpoints of the link $\xi = 0$ and $\xi = l$ in non-homogenous boundary conditions (equivalent to (10)) to eliminate higher-order temporal derivatives and obtain transformed boundary equations (equivalent to (36)). Then, a model transformation function is obtainable, satisfying transformed boundary conditions (equivalent to (46)). The model transformation should also satisfy homogenous boundary conditions.

Theorem 2. The transformed mathematical model (54)–(58) as well as the boundary conditions (38)–(40) express the flexible system dynamics (8)–(12) in homogenized form.

$$\begin{aligned}&\Big\{I_m + Ml^2 + Mz^2(l) - \rho A\frac{l^3}{3} \\ &\qquad + \rho A\int_0^l [z^2(\xi) - 2z(\xi)\nu(\xi) \\ &\qquad + \nu^2(\xi)]\, d\xi\Big\}\ddot{\theta} - Mlz_{tt}(l) + h_1 \\ &\qquad = \tau + u\left[l - \rho A p_2 + \rho A\kappa\dot{\theta}^2 p_1\right]\end{aligned} \tag{54}$$

$$z_{tt}(\xi) + [\gamma(\xi)\kappa g \sin\theta + \xi]\ddot{\theta} + h_2 = u \tag{55}$$

$$\begin{aligned} h_1 = &-2M\omega(l)\omega_t(l) + \rho A\kappa g\cos\theta\, c_1 + \frac{1}{2}mgl\cos\theta \\ &+ Mgl\cos\theta + Mgz(l)\sin\theta \\ &- \rho Ag\cos\theta\, p_2 \\ &+ \rho A\int_0^l \Big\{2z(\xi)z_t(\xi)\dot\theta \\ &- 2z(\xi)\gamma(\xi)k\dot u\dot\theta \\ &+ 2z(\xi)\gamma(\xi)\kappa g\dot\theta^2\sin\theta \\ &- 2v(\xi)z_t(\xi)\dot\theta + 2v^2(\xi)\dot\theta + \dot\theta^2\xi z(\xi) \\ &- \frac{1}{\kappa}\xi z_{\xi\xi\xi\xi}(\xi)\Big\}d\xi \end{aligned} \tag{56}$$

$$h_2 = -z(\xi)\dot\theta^2 + \frac{1}{\kappa}z_{\xi\xi\xi\xi}(\xi) - \gamma_1 e^{-p\xi}g\cos\theta \tag{57}$$

$$u = \gamma(\xi)k\ddot u - \left[\gamma_1 e^{-p\xi} + \gamma(\xi)k\dot\theta^2\right]u \tag{58}$$

Proof. The proof is detailed in Appendix C.

V. Solvability and Implementation of a Homogenized Model

The transformed model (54)–(58) with homogenized boundary conditions (38)–(40) allows for the implementation of semi-analytical solutions—for example, the Galerkin method or the Rayleigh–Ritz method [3]—instead of intensive numerical solvers, such as those based on finite elements. Such methods are based on obtaining an orthogonal basis for displacement states. Homogenized boundary conditions allow the straightforward calculation of an orthogonal basis for the transformed model as a function of $z(\xi)$ instead of $\omega(\xi)$. As a result, the model, as well as the corresponding control law (34), can be implemented by assigning a discretized expression of displacement (59) in (54)–(58).

$$z(\xi,t) = \sum_{i=1}^{n_m}\eta_i(t)\phi_i(\xi) \tag{59}$$

The standard choice for orthogonal basis $\phi_i(\xi)$ is implemented as follows:

$$\begin{aligned} \phi_i(\xi) = c_{1i}(\cos\beta_i\xi + \cosh\beta_i\xi) + c_{2i}(\cos\beta_i\xi - \\ \cosh\beta_i\xi) + c_{3i}(\sin\beta_i\xi + \sinh\beta_i\xi) + c_{4i}(\sin\beta_i\xi - \\ \sinh\beta_i\xi). \end{aligned} \tag{60}$$

Substituting in homogenized boundary conditions (38)–(40), coefficient c_{ij} and natural frequency β_i are calculated based on (61)–(67) for the transformed model.

$$c_{1i} = c_{3i} = 0 \tag{61}$$

$$\begin{bmatrix}\mathfrak{B}_{11} & \mathfrak{B}_{12}\\ \mathfrak{B}_{21} & \mathfrak{B}_{22}\end{bmatrix}\begin{bmatrix}c_{2i}\beta_i^2\\ c_{4i}\beta_i^2\end{bmatrix} = \begin{bmatrix}0\\0\end{bmatrix} \tag{62}$$

$$\mathfrak{B}_{11} = -\cos\beta_i\xi - \cosh\beta_i\xi \tag{63}$$

$$\mathfrak{B}_{12} = -\sin\beta_i\xi - \sinh\beta_i\xi \tag{64}$$

$$\begin{aligned} \mathfrak{B}_{21} = \beta_i^2\cos\beta\xi - \beta_i^2\cosh\beta_i\xi + \frac{\rho A}{M}\beta_i\sin\beta_i\xi \\ - \frac{\rho A}{M}\beta_i\sinh\beta_i\xi \end{aligned} \tag{65}$$

$$\begin{aligned} \mathfrak{B}_{22} = \beta_i^2\sin\beta_i\xi - \beta_i^2\sinh\beta_i\xi - \frac{\rho A}{M}\beta_i\cos\beta\xi \\ - \frac{\rho A}{M}\beta_i\cosh\beta\xi \end{aligned} \tag{66}$$

$$\begin{aligned} \int_0^l \phi_i^2\, d\xi = c_{2i}^2\int_0^l \Big[&\cos\beta_i\xi - \cosh\beta_i\xi \\ &- \frac{\cos\beta_i\xi + \cosh\beta_i\xi}{\sin\beta_i\xi + \sinh\beta_i\xi}(\sin\beta_i\xi \\ &- \sinh\beta_i\xi)\Big]^2 d\xi = 1 \end{aligned} \tag{67}$$

This leads to the calculation of the coefficients as:

$$c_{4i} = -\frac{\cos\beta_i\xi + \cosh\beta_i\xi}{\sin\beta_i\xi + \sinh\beta_i\xi}c_{2i}, \tag{68}$$

$$\begin{aligned} c_{2i} = \Big\{\int_0^l \Big[&\cos\beta_i\xi + \cosh\beta_i\xi - \frac{\cos\beta_i\xi + \cosh\beta_i\xi}{\sin\beta_i\xi + \sinh\beta_i\xi}(\sin\beta_i\xi - \\ &\sinh\beta_i\xi)\Big]^2 d\xi\Big\}^{-\frac{1}{2}}. \end{aligned} \tag{69}$$

Hence, $\phi_i(\xi)$ is obtainable based on homogenized boundary conditions. Substituting (59) in transformed model (48)–(52) with homogenized boundary conditions (38)–(40), the states $\eta_i(t)$ are calculable by solving their corresponding ODEs. $\eta_i(t)$ is calculable by substituting the discretized expression of distributed system state $z(\xi,t) = \sum_{i=1}^{n_m}\eta_i(t)\phi_i(\xi)$ in transformed model (54)–(58) using assumed mode methods [3]. On this basis, (54) is transformed to a corresponding equation with states of $\eta_i(t)$ and θ, and (55) is transformed to n_m ordinary differential equations by substituting $z(\xi,t) = \sum_{i=1}^{n_m}\eta_i(t)\phi_i(\xi)$ in (55), multiplying it in $\phi_j(\xi), j = 1,\dots n_m$, and integrating the expressions over the length of the beam. This results in $n_m + 1$ equations for $n_m + 1$ states, which is instantly solvable. This leads to the calculation of $z(\xi,t)$ based on (59).

Finally, the original displacements are obtained as one-to-one mapping, according to (37).

Remark 8. Coefficients c_{ij} are not readily calculable using original boundary conditions, as the right-hand side term in (62) is not a zero vector. Hence, non-trivial solutions and natural frequencies for β_i and $\phi_i(\xi)$ are not calculable analytically.

Alternatively, model transformation (37) may be used to obtain displacement data through the length of the flexible beam without dependency on input torque when n_m measurements corresponding to endpoint displacement and its time derivatives are available. As $z(l) = \sum_{i=1}^{n_m}\eta_i(t)\phi_i(l) = \omega(l)$ and $\sum_{i=1}^{n_m}\eta_i(t)\frac{d^n\phi_i(l)}{d\xi^n} = \frac{\partial\omega^n(l)}{\partial\xi^n}$, n_m is the number of η_is given n_m equations corresponding to measurements $\omega(l), \omega_\xi(l), \dots, \frac{\partial^{n_m}\omega(l)}{\partial\xi^n}$ for $n = 1,\dots,n_m$.

$$\boldsymbol{\phi}\underline{\boldsymbol{\eta}} = \underline{\boldsymbol{\omega}}_l \tag{70}$$

$$\boldsymbol{\phi} = \begin{bmatrix}\phi_1(l) & \cdots & \phi_{n_m}\\ \vdots & \ddots & \vdots \\ \dfrac{d^{n_m}\phi_1(l)}{d\xi^{n_m}} & \cdots & \dfrac{d^{n_m}\phi_{n_m}(l)}{d\xi^{n_m}}\end{bmatrix} \tag{71}$$

$$\underline{\boldsymbol{\eta}} = \begin{bmatrix}\eta_1\\ \vdots \\ \eta_{n_m}\end{bmatrix} \tag{72}$$

$$\underline{\boldsymbol{\omega}}_l = \begin{bmatrix}\omega(l)\\ \vdots \\ \dfrac{\partial^{n_m}\omega(l)}{\partial\xi^n}\end{bmatrix} \tag{73}$$

Equation (70) is solvable for $\underline{\boldsymbol{\eta}}$. Hence, $\omega(\xi)$ is obtainable as follows:

$$\omega(\xi) = \sum_{i=1}^{n_m} \eta_i(t)\phi_i(\xi) - \nu(\xi). \quad (74)$$

By calculating $\omega(\xi)$, all required feedback information for calculating the control input (34) is available.

Remark 9. Solution (74) is more convenient to implement for boundary control schemes than substituting (59) in the transformed model, as boundary feedback corresponding to $\omega(l)$ is measured to obtain error-based terms and is more accurate to obtain than time derivatives of the boundary input.

Remark 10. As displacement mapping (74) is differentiable, derivatives of displacement $\omega(\xi)$ are analytically calculable, which eliminates the need for potentially inaccurate numerical differentiation.

Summarizing the methodology presented in Sections 3–5, the procedure for implementing the boundary controller and obtaining the semi-analytical solution is presented as an algorithm in Table 1 and in block diagram form in Fig. 2.

VI. Results and Discussion

In this section, the implementation of the proposed solution method is discussed, and the response of the closed-loop system to the proposed control strategy is investigated. The mechanical and geometric properties of the simulated system, as well as the fixed decision variables used in the estimation and control scheme, are described in Table 2. As Euler–Bernoulli beam theory is used in this study to model the flexible beam, the manipulator must feature a length-to-thickness ratio of 10 or more [3].

The control and estimation efficiency is investigated to track the harmonic reference joint angle signal $(x_{l,r}, y_{l,r}) = (l\cos\theta_r\,[m], l\sin\theta_r\,[m])$, where $\theta_r = a_r\cos\omega_r\,[rad]$ with $a_r = 0.20\,[rad]$ and $\omega_r = 3.00\,[rad/s]$. The time-varying properties of the control scheme described in Table 1 are assigned online so that they satisfy the corresponding mathematical conditions obtained in Section III. An initial tip displacement of $\omega_0(l) = 0.050\,[m]$ is considered. In online calculations, it is set that $\delta_1 = 0.001|-e_1\nu_1|$ and $\delta_2 = 0.001\left|-e_2\nu_2 - m_f\nu_{0_1} - h_f\right|$ to ensure decay of the Lyapunov function with respect to (A.21). The sampling time in numerical simulations is set to $T = 0.001\,[s]$.

TABLE 1
IMPLEMENTATION OF A BOUNDARY CONTROLLER BASED ON A SEMI-ANALYTICAL PDE SOLUTION

// Initial configuration	
Assign endpoint trajectory reference (x_r, y_r)	
(i) Set control parameters for error λ_θ and λ_ω	(24)
(ii) Assign weight to mitigation of flexibility effects throughout the length of the flexible beam based on α and β	(B.4, B.8)
(iii) Calculate model transformation coefficient $\gamma(\xi)$	(53)
(iv) Assign uncertainty bounds for $\underline{\boldsymbol{s}}$ and define $\underline{\boldsymbol{\lambda}}_Q$	(29, B.30)
// Online measurements	
(v) Obtain joint-angle measurement at current sample θ	
(vi) Endpoint deflection measurements $\omega(l)$, $\omega_t(l)$, and $\omega_{\xi\xi\xi}(l)$	
// PDE-based controller: sample n	
(vii) Obtain error vector $\underline{\boldsymbol{e}}$	(24)
(viii) Calculate temporal state vector $\underline{\boldsymbol{\eta}}$	(70)
(ix) Obtain transformed distributed variable $z(\xi)$	(59)
(x) Obtain model transformation variable $\nu(\xi)$ based on boundary inputs, nonlinear terms, and $\gamma(\xi)$	(52)
(xi) Calculate distributed states $\omega(\xi)$	(74)
(xii) Calculate online control terms $\underline{\boldsymbol{\gamma}}$, $\underline{\boldsymbol{\gamma}}_0$, $\underline{\boldsymbol{\nu}}$, and $\underline{\boldsymbol{\nu}}_0$	(25, 26, B.17, B.18)
(xiii) Calculate distributed terms m_f and h_f	(B.14, A.15)
(xiv) Calculate $\widehat{\boldsymbol{\mathcal{M}}}$ and $\widehat{\boldsymbol{\hbar}}$ based on stages vii–xiii	(B.21, 34)
(xv) Obtain control signal $\underline{\boldsymbol{u}}$ for current sample	(34)
(xvi) Updated estimated system parameters vector	(35)
// Implementation of control action	
(xvii) Exert $\underline{\boldsymbol{u}}$ to dynamical system	(15,54)
(xviii) Increase n to $n+1$ and go to (iii)	

TABLE 2
MECHANICAL, GEOMETRIC, AND NUMERICAL PROPERTIES OF THE CLOSED-LOOP SYSTEM

Parameter	Value	Parameter	Value
$\boldsymbol{\rho A}$	$0.40\ [kg/m]$	α	5.00
$\boldsymbol{EI}$	$5.00e3\ [N.m^2]$	β	1.00
$\boldsymbol{l}$	$4.50\ [m]$	$\lambda_\theta, \lambda_\omega$	5.00
$\boldsymbol{M}$	$2.00\ [kg]$	g	$9.81\ [m/s^2]$

Control law (34) is implemented, which requires boundary measurements $\omega(l)$, $\omega_t(l)$, and $\omega_{\xi\xi\xi}(l)$ as well as joint measurements θ and $\dot{\theta}$. To obtain the integrated terms featuring the distributed states in (34)—that is, the terms in the form of $\int_0^l f\left[\omega(\xi), \omega_t(\xi), \omega_\xi(\xi), \omega_{\xi\xi\xi\xi}(\xi)\right] d\xi$—(74) is used, which enables computationally efficient calculation of $\omega(\xi)$ and higher-order derivatives with respect to boundary measurements and model transformation (37). Initially, closed-loop system performance without any parametric uncertainty is evaluated. Subsequently, the effects of parametric uncertainty on the control response are investigated.

The results of the numerical simulation of the closed-loop system for the aforementioned configuration implanted in the MATLAB® environment using codes without any external solvers or MATLAB® toolboxes—for example, FEA solvers—are shown in Figs. 3–5.

Fig. 3 shows the convergence of the closed-loop system's response to the associated reference signals, which are guaranteed using stability-proofed PDE-based control analysis. As described in Fig. 4, the use of the proposed boundary control scheme results in the elimination of undesired deflection effects throughout the length of the flexible beam. Fig. 5 depicts the control inputs—that is, the joint input torque and the boundary input force—which retain their bounded values. A calculation time of $2.73\ [s]$ over the simulation length of $5.00\ [s]$ was recorded using the proposed semi-analytical solution. This indicates the implementability of the proposed schemes in real-time applications.

In Fig. 6, the performance and applicability of the control scheme for discontinuous piece-wise reference signal $\theta_r = a_r\ sign\ (\cos \omega_r)[rad]$ with $a_r = -0.30\ [rad]$ and $\omega_r = 2.00\ [rad/s]$ is investigated to study system performance in the case of instantaneous excitations. As depicted in Fig. 6, the controller maintains tracking performance and converges to a new angle reference value in finite time. Furthermore, endpoint displacement is mitigated in each interval.

Fig. 7 investigates the feasibility of the adaptive scheme for the closed-loop system considering the uncertainty of system parameter vector $\underline{\boldsymbol{s}}$. To this end, the system response is investigated for cases with 30%, 60%, and 90% additive uncertainty in $\underline{\boldsymbol{s}}$, which is equivalent to $\underline{\hat{\boldsymbol{s}}} = 1.3\underline{\boldsymbol{s}}$, $\underline{\hat{\boldsymbol{s}}} = 1.6\underline{\boldsymbol{s}}$, and $\underline{\hat{\boldsymbol{s}}} = 1.9\underline{\boldsymbol{s}}$, respectiely. The results are compared with the deterministic system. In all cases, the upper uncertainty bound of $\underline{\boldsymbol{s}}_h = 1.3\,\underline{\hat{\boldsymbol{s}}}$ and lower uncertainty bound $\underline{\boldsymbol{s}}_l = 0.8\,\underline{\boldsymbol{s}}$ are assigned. As depicted in Fig. 7, the closed-loop system maintains a bounded response in all investigated cases and successfully mitigates joint angle tracking error and endpoint displacement, despite the presence of additive parametric uncertainty. As expected, higher error values are observed in cases where higher values of parametric uncertainty are considered. This corresponds to an increased initial error for systems with larger parametric uncertainty and is eliminated with time.

The performance of the controller is compared with that of a standard potential-differential strain feedback controller (PDS) [32], [37], which uses error feedback for the joint angle, endpoint displacement, and its higher-order derivatives to mitigate the mentioned effects. On this basis, inputs are assigned as $\tau = -k_{p,\theta} e_1 - k_{d,\theta} \dot{e}_1$ and $u = -k_{p,\omega}\omega(l) - k_{d,\omega}\dot{\omega}(l) - k_{s,\omega}\omega_{\xi\xi\xi}(l)$. Based on the manipulator configuration, for the PDS controller to demonstrate satisfactory performance, a high-gain approach must be attained. Controller gains are set as $k_{p,\theta} = k_{p,\omega} = 2000$, $k_{d,\theta} = k_{d,\omega} = 200$, and $k_{s,\omega} = 5$. The results of the comparisons are depicted in Fig. 8.

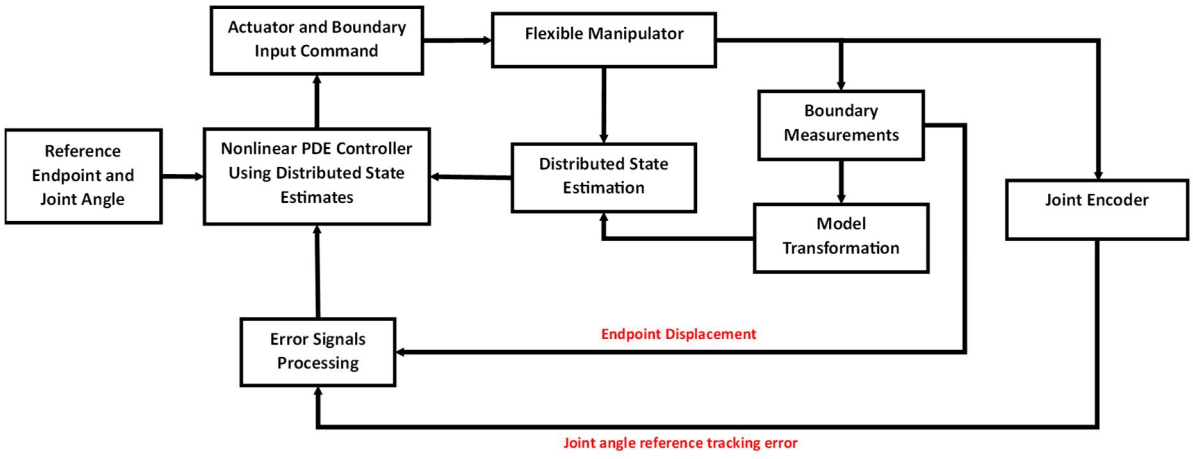

Fig. 2. Block diagram of closed-loop system featuring distributed state estimation, nonlinear PDE controller, and required feedback

As indicated, the main difference is that the adaptive model-based boundary controller (AMBC) proposed in this study ensures gradual mitigation of the joint angle tracking error and endpoint displacement, as indicated by stability analysis, while the PDS controller maintains the boundedness of states in an area around the origin, as the variable dynamic terms and coupling effects are not considered in its design. Specific modifications for the PDS controller may be conducted to include the aforementioned effects. Furthermore, the performance of the PDS controller is highly dependent on controller gain, and the selection of unsuitable gains may result in instability in the system when prior stability analysis is not conducted. In the AMBC controller, the selection of control parameters is conducted according to the provided guidelines, as referenced in Table 1. Any control parameter selected within the feasible region maintains boundedness and stability, although they affect control performance. A potential drawback of an AMBC controller is the complexity of the model-based design and distributed state measurement, which are not required in a PDS controller.

To verify the precision of the proposed distributed state estimation scheme and the corresponding model transformation in practice, the experimental setup described in Fig. 9 featuring a flexible manipulator with non-homogenous boundary conditions is used. The experimental setup features a long-reach flexible beam, payload mass, and hydraulic input. The manipulator is equivalent to the one-link flexible manipulator depicted in Fig. 1 and is described by mathematical model (8)–(12) when the assigned boundary input force is equal to zero. Gravity effects still affect the boundary conditions of the mechanism due to the payload installed at the endpoint of the manipulator. Hence, the mechanism features non-homogenous boundary conditions in the form of (36) as $\omega_{\xi\xi\xi\xi}(l) + \frac{\rho A}{M}\omega_{\xi\xi\xi}(l) = \kappa g \cos\theta$, which prevents the use of straightforward analytical PDE solutions based on separation-of-variables. Therefore, the model transformation proposed in

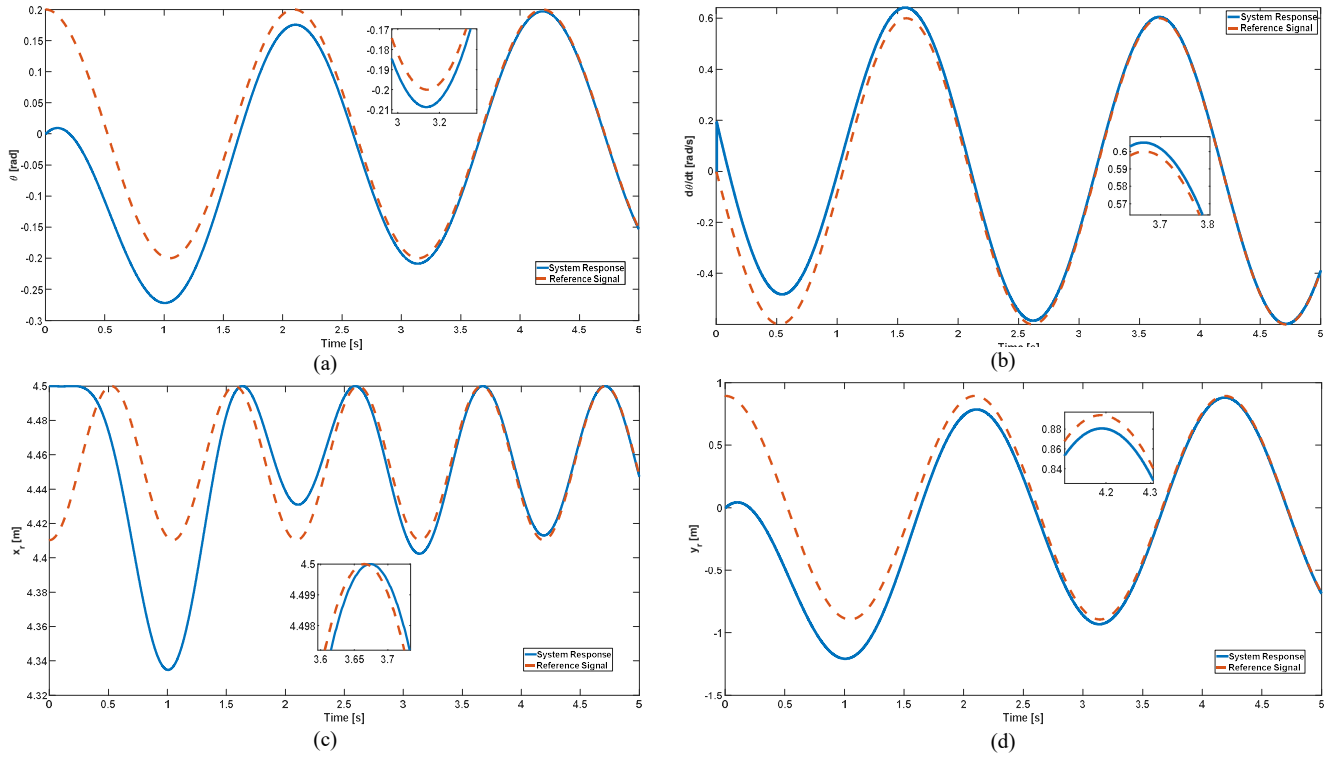

Fig. 3. Tracking performance of controller: (a) Joint angle; (b) Joint velocity; (c) Endpoint horizontal position; (d) Endpoint vertical position.

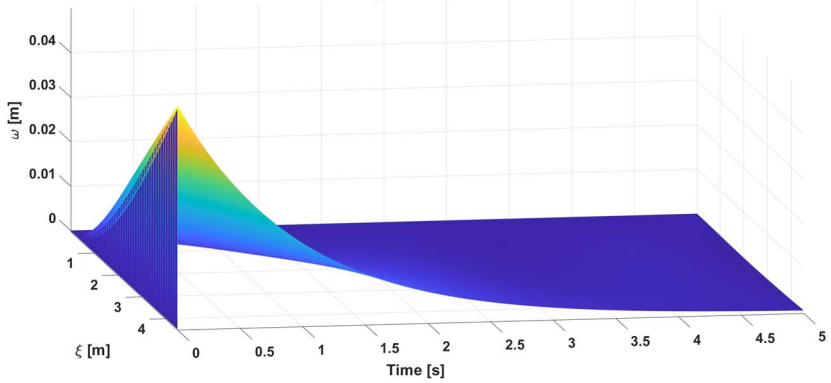

Fig. 4. Displacement of flexible link over time.

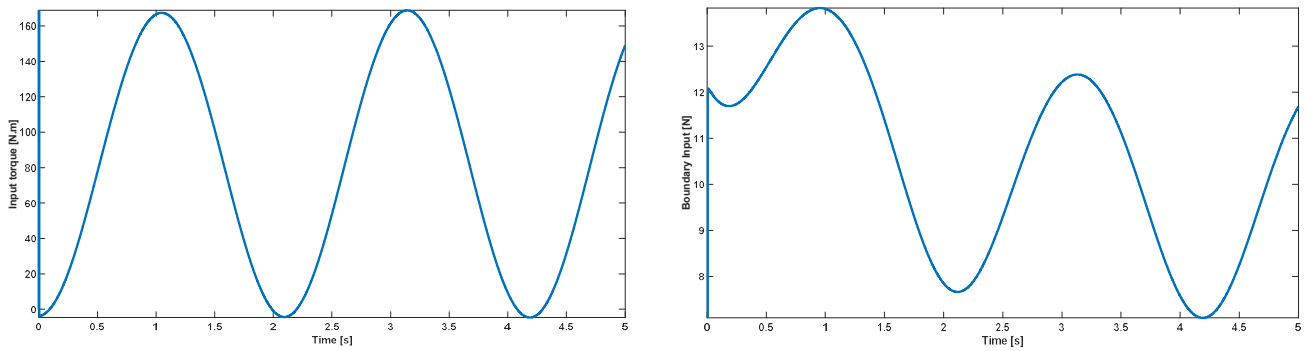

(a) (b)

Fig. 5. Control input signals: (a) Joint torque; (b) Boundary input force.

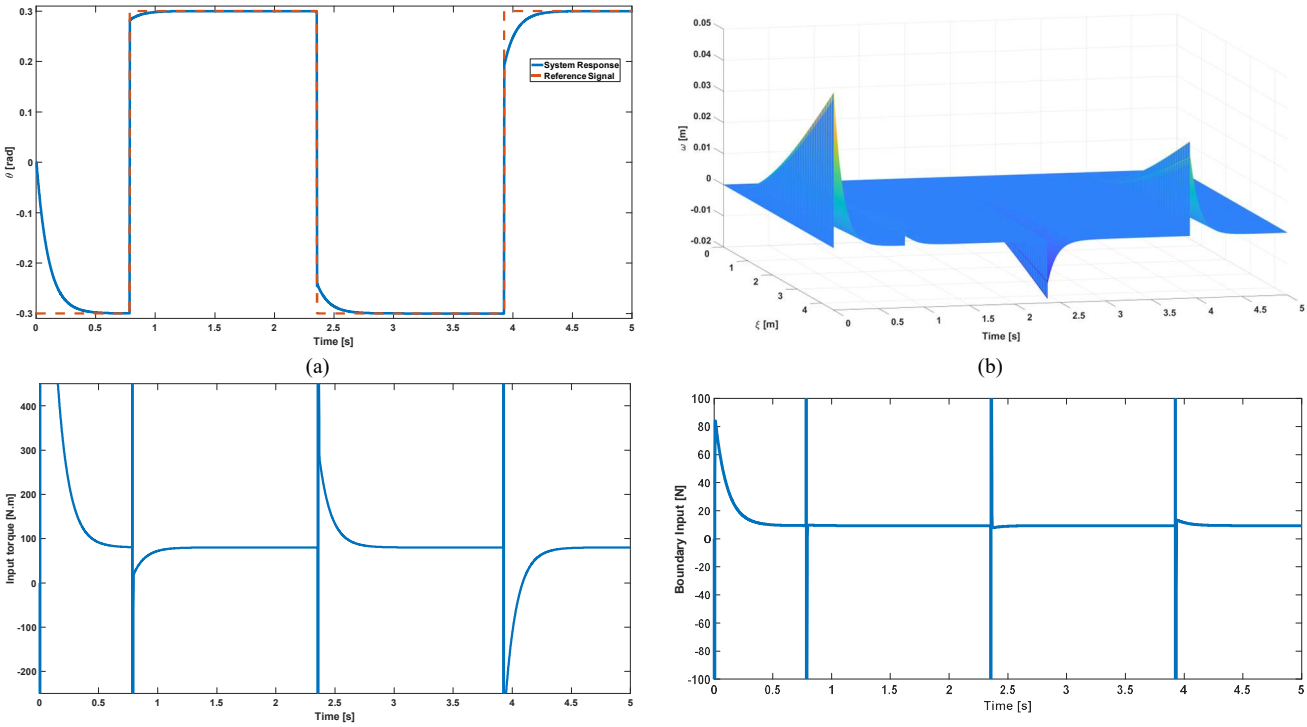

(a) (b)

(c) (d)

Fig. 6. Controller performance for a discontinuous piece-wise reference signal: (a) Joint angle; (b) Displacement of flexible link over time; (c) Joint torque; (d) Boundary input force.

this study is used to obtain distributed states throughout the length of the manipulator, in accordance with the conducted numerical simulations and the procedure detailed in Sections IV and V of the manuscript. To this end, the displacement of the manipulator endpoint located at $\xi = 4.63\ [m]$ as well as two select elements at $\xi = 2.32\ [m]$ and $\xi = 3.41\ [m]$ have been calculated based on comparisons between the position measurements of the elements and the position of the same elements in a rigid manipulator, according to (2) and (3). Ground truth measurements for the beam are obtained using three camera markers installed on the beam with the OptiTrack® Prime 17W position motion capture system. The joint angle is measured using an absolute encoder with 18-bit per revolution resolution. A hydraulic actuator exerts system input F_h to the element located at $\xi_h = 0.35\ [m]$, which acts as joint torque $\tau = F_h \xi_h$ when forgoing longitudinal displacement of the beam. The flexible manipulator features geometric and mechanical properties of $I = 3.51e-4\ [m^4]$, $E = 2.10e11\ [Pa]$, and $\rho = 7850.00\ [\frac{kg}{m^3}]$. The payload with $M = 20.00\ [kg]$ is installed at the endpoint of the manipulator.

To verify the displacement estimation using the proposed model, the endpoint displacement is measured for an assigned trajectory, as depicted in Fig. 10, and is subsequently used to obtain the time function $\underline{\boldsymbol{\eta}}$ according to (70). $\nu(\xi)$ is obtained according to (52), and the estimated displacement values are calculated for the camera markers placed at $\xi = 2.32\ [m]$ and $\xi = 3.41\ [m]$, based on (74). Displacement values obtained using the camera measurements for the same elements are considered ground truth and are compared with values obtained using mapping (74) in Fig. 11, which expresses the precision of the proposed displacement estimation method. With respect to directly distributed measurements using a limited number of sensors, obtaining displacement values for samples that do not correspond to measurement points is improved using mapping (74). This is highlighted in Fig. (11.d), which compares the

estimated displacement of the measurement points at $\xi_1 = 2.32\ [m]$ and $\xi_2 = 3.41\ [m]$ obtained by mapping (74) with estimated displacements calculated based on the interpolation of measurement data. For this comparison, the interpolation of measurements between $\xi = 0\ [m]$ and $\xi_2 = 3.41\ [m]$ is used to estimate displacement for $\omega(\xi_1 = 2.32\ )$, and the interpolation of measurements between $\xi_1 = 2.32\ [m]$ and $\xi = l$ is used to estimate displacement for $\omega(\xi_2 = 3.41)$. The results highlight the potential inaccuracy of using distributed measurements to estimate the displacement of flexible links at points other than measurement samples, which results in significant inaccuracy when calculating terms featuring the integration of distributed states.

In this experiment, estimation error values are primarily caused by the deformation of a long-reach flexible manipulator in its original form, which does not correspond to a fully rigid link with $(r_{x,\xi}, r_{y,\xi}) = (\xi\cos\theta, \xi\sin\theta)$. Longitudinal displacement of the flexible beam is also often significant due to the length of the manipulator. Error estimation may be improved by incorporating models that feature longitudinal displacement effects [38]. Inaccuracies in system parameters and measurement biases are also potential error sources. Fig. 12 describes the results of the density amplitude analysis per frequency for the experimental data and indicates the applicability of the proposed displacement calculation scheme for different operating frequencies, including the two excited natural frequencies.

V. Conclusion

This paper details a novel design and implementation procedure for the boundary control of a flexible manipulator, enabling high-speed calculations based on a semi-analytical solution for the corresponding PDEs. This is conducted by obtaining a model transformation to homogenize the original

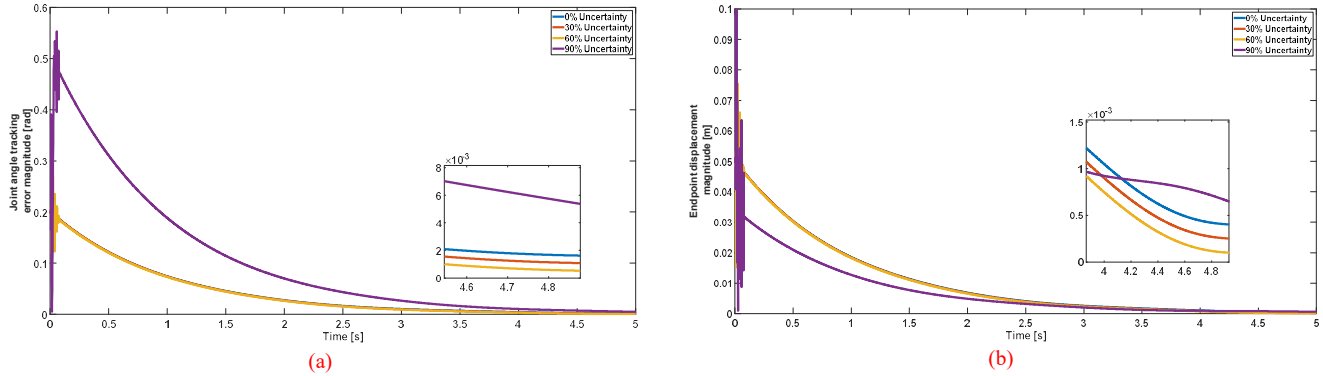

Fig. 7. Adaptive controller tracking performance analysis: (a) Joint angle tracking magnitude; (b) Endpoint displacement magnitude.

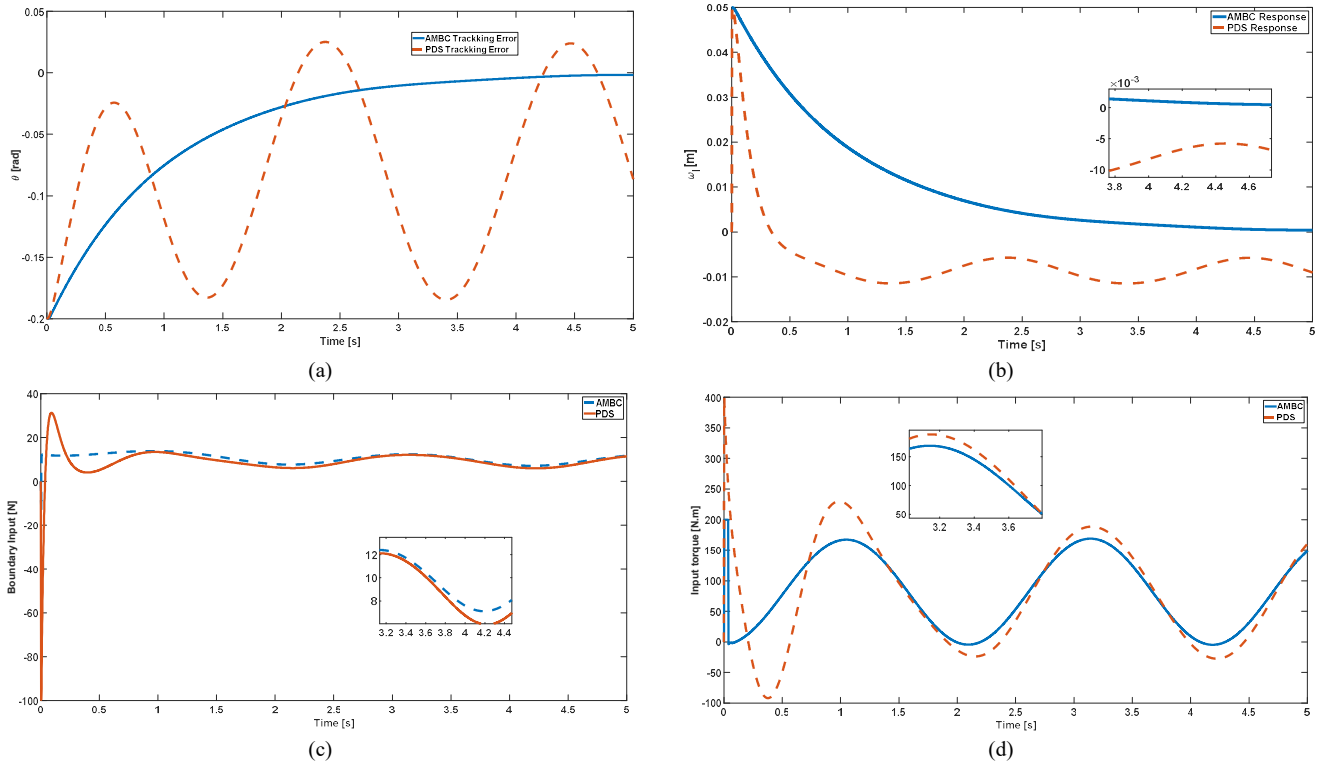

Fig. 8. Comparative analysis of AMBC and PDS controllers: (a) Joint angle; (b) Displacement of flexible link over time; (c) Joint torque; (d) Boundary input force.

PDE model, which can be used in combination with boundary measurements to obtain distributed states—that is, displacement values and their higher-order temporal and spatial derivatives—throughout the length of a flexible beam in a convenient manner, despite the existence of nonlinear gravity and input terms. Distributed state values are used to obtain the boundary control law, resulting in precise endpoint trajectory tracking based on the elimination of undesired deflection values and the tracking of joint angle states. The presented control strategy is robust to parametric uncertainty due to its adaptive design. The effectiveness of the model transformation scheme for the recovery of distributed states is demonstrated based on experimental data, and numerical calculations are used to indicate high-speed computations corresponding to the PDE control scheme. Future research opportunities include the investigation of longitudinal displacement effects, unstructured model uncertainties, and the extension of the proposed model to multibody flexible systems.

ACKNOWLEDGMENTS

Equipment provided by the Centre for Immersive Visual Technologies (CIVIT) was used in this research.

APPENDIX

Appendix A. Variation terms for the dynamic model

To obtain the dynamic model, variations in energy and work terms (5)–(7) are calculated. Initially, a time derivative of the element position vector is calculated as follows:

$$\dot{r}_{x,\xi} = -\xi\dot{\theta}\sin\theta - \dot{\omega}(\xi)\sin\theta - \omega(\xi)\dot{\theta}\cos\theta, \quad \text{(A.1)}$$

$$\dot{r}_{y,\xi} = \xi\dot{\theta}\cos\theta + \dot{\omega}(\xi)\cos\theta - \omega(\xi)\dot{\theta}\sin\theta. \quad \text{(A.2)}$$

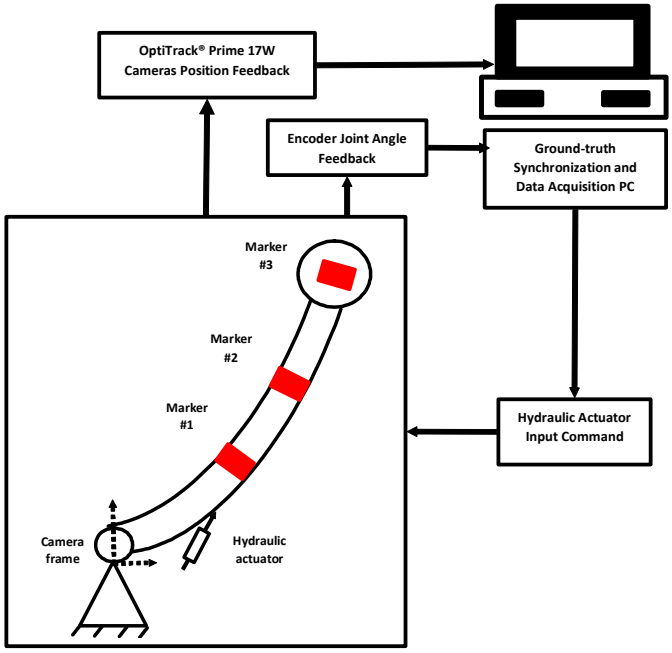

(a)

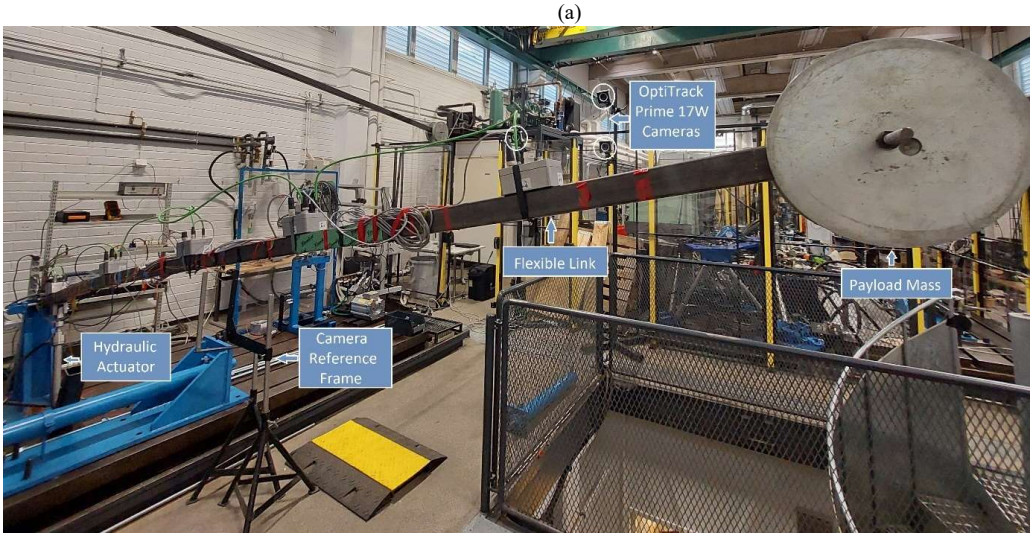

(b)

Fig. 9. (a) Schematic description of the set-up; (b) Flexible manipulator setup with camera position feedback.

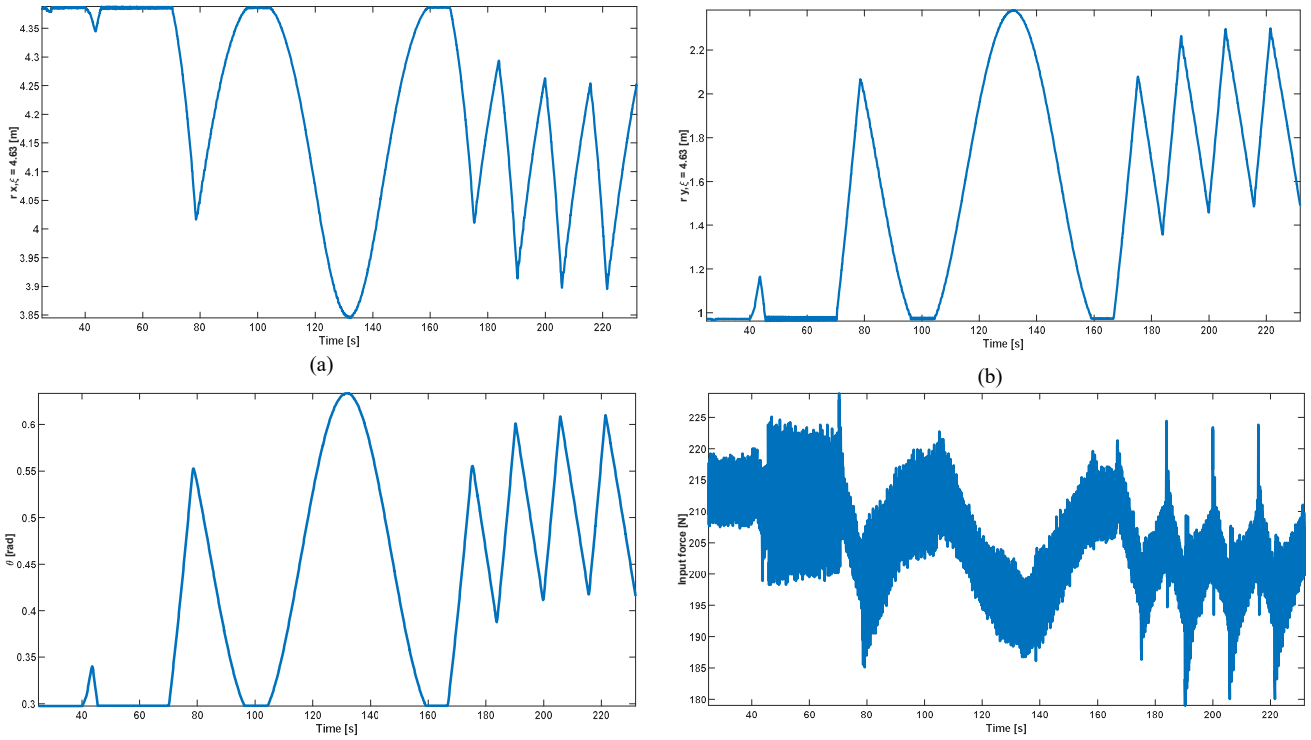

Fig. 10. Endpoint trajectory of the flexible manipulator obtained using camera measurements: (a) $r_{x,l}$; (b) $r_{y,l}$; (c) Joint angle; (d) Hydraulic input.

Substituting (A.1) and (A.2) in (5), the kinetic energy term is expanded as follows:

$$T = \frac{1}{2}\rho A \int_0^l \dot{\bar{\boldsymbol{r}}}_\xi^T \dot{\bar{\boldsymbol{r}}}_\xi \, d\xi + M\dot{\bar{\boldsymbol{r}}}_l^T \dot{\bar{\boldsymbol{r}}}_l = \frac{1}{2} I_m \dot{\theta}^2 + \frac{1}{2}\rho A \int_0^l \left[\dot{\omega}^2(\xi) + \omega^2(\xi)\dot{\theta}^2 + 2\xi\dot{\theta}\dot{\omega}(\xi)\right] d\xi + \frac{1}{2} M\left[l^2\dot{\theta}^2 + \dot{\omega}^2(l) + \omega^2(l)\dot{\theta}^2 + 2l\dot{\theta}\dot{\omega}(l)\right]. \tag{A.3}$$

Applying the variation operator to (A.3) and then using integration-by-parts results in:

$$\begin{aligned}\delta \int_{t_1}^{t_2} T\, dt \; &= \int_{t_1}^{t_2} \Big\{ I_m \dot{\theta}\delta\dot{\theta} + \rho A \int_0^l \big[\omega_t(\xi)\delta\omega_t + \omega(\xi)\dot{\theta}^2\delta\omega(\xi) + \omega^2(\xi)\dot{\theta}\delta\dot{\theta} + \xi\dot{\theta}\delta\omega_t(\xi) + \xi\omega_{tt}(\xi)\delta\dot{\theta}\big]\, d\xi + M\big[l^2\dot{\theta}\delta\dot{\theta} + \omega_t(l)\delta\omega_t(l) + \omega(l)\dot{\theta}^2\delta\omega(l) + \omega^2(l)\dot{\theta}\delta\dot{\theta} + l\dot{\theta}\delta\omega_t(l) + l\omega_t(l)\delta\dot{\theta}\big]\Big\} dt = \int_{t_1}^{t_2} \Big\{ \Big\{ -I_m\ddot{\theta} - Ml^2\ddot{\theta} - M\omega^2(l)\ddot{\theta} - 2M\omega(l)\omega_t(l)\dot{\theta} - Ml\omega_{tt}(l) + \rho A \int_0^l \big[-2\omega(\xi)\omega_t(\xi)\dot{\theta} - \omega^2(\xi)\ddot{\theta} - \xi\omega_{tt}(\xi)\big]\, d\xi \Big\}\delta\theta + \Big\{\rho A \int_0^l \big[-\omega_{tt}(\xi) + \omega(\xi)\dot{\theta}^2 - \xi\ddot{\theta}\big]\, d\xi\Big\}\delta\omega(\xi) + \big[-M\omega_{tt}(l) + M\omega(l)\dot{\theta}^2 - Ml\ddot{\theta}\big]\delta\omega(l)\Big\} dt. \end{aligned} \tag{A.4}$$

Variations in potential energy (6) are calculated using consecutive integration-by-parts.

$$\begin{aligned}\delta \int_{t_1}^{t_2} V\, dt = \int_{t_1}^{t_2} \Big\{ &\frac{1}{2} mgl\cos\theta\,\delta\theta + Mgl\cos\theta\,\delta\theta + Mg\cos\theta\,\delta\omega(l) - Mgsin\,\theta\omega(l)\delta\theta + EI\int_0^l \omega_{\xi\xi}\delta\omega_{\xi\xi}\, d\xi\Big\} dt = \int_{t_1}^{t_2} \Big\{ \Big[\frac{1}{2} mgl\cos\theta + Mgl\cos\theta - Mgsin\,\theta\omega(l)\Big]\delta\theta + \big[-EI\omega_{\xi\xi\xi} + Mg\cos\theta\big]\delta\omega(l) + EI\omega_{\xi\xi}\delta\omega'(l) - EI\omega_{\xi\xi}\delta\omega'(0) + EI\omega_{\xi\xi\xi}\delta\omega(0) + EI\int_0^l \omega_{\xi\xi\xi\xi}\, d\xi\delta\omega(\xi)\Big\} dt, \end{aligned} \tag{A.5}$$

To calculate δW according to (7), $\delta\bar{\boldsymbol{r}}_l$ is expressed as:

$$\delta\bar{\boldsymbol{r}}_l = \begin{bmatrix} [-l\,sin\,\theta - \omega(l)\sin\theta]\delta\theta - \sin\theta\,\delta\omega(l) \\ [l\,cos\,\theta + \omega(l)\cos\theta]\delta\theta + \cos\theta\,\delta\omega(l) \end{bmatrix}. \tag{A.6}$$

Substituting (A.6) in (7) results in:

$$\delta W = (\tau + ul)\delta\theta \; + u\delta\omega(l). \tag{A.7}$$

Finally, (A.4), (A.5), and (A.7) are substituted in extended Hamilton principle $\delta(T - V + W) = 0$. Setting the term multiplied in $\delta\theta$ to zero directly leads to (8), and setting the term multiplied in $\delta\omega(\xi)$ results in (9). Boundary conditions (10)–(12) are obtained by setting terms multiplied in $\delta\omega(0)$, $\delta\omega_\xi(0)$, $\delta\omega(l)$, and $\delta\omega_\xi(l)$ to zero.

Appendix B. Proof of Theorem 1

Candidate Lyapunov Functional (CLF) (B.1) is investigated to obtain the control law.

$$V = V_t + V_f + V_s \tag{B.1}$$

$$V_f = V_b + V_e, \tag{B.2}$$

where V_t, V_f, and V_s represent the components of CLF corresponding to joint angle tracking, the elimination of link flexibility, and parameter adaptation, respectively. V_f consists of the effects corresponding to the length of the flexible beam, V_b, as well as those of the endpoint deflections, V_e.

$$V_t = \frac{1}{2} e_1^2 \tag{B.3}$$

$$V_b = \frac{1}{2}\int_0^l \left[\alpha\omega_t^2(\xi) + \alpha\frac{EI}{\rho A}\omega_{\xi\xi}^2(\xi) + \beta\xi\omega_t(\xi)\omega_\xi(\xi)\right] d\xi \tag{B.4}$$

$$V_e = \frac{1}{2} e_2^2 \tag{B.5}$$

Coefficients $\alpha \in \mathbb{R}^+$ and β are decision variables, satisfying conditions that are obtained later.

Component V_s is defined with respect to parameter estimation error.

$$V_s = \frac{1}{2}\underline{\tilde{\mathbf{s}}}^T\underline{\tilde{\mathbf{s}}} \tag{B.6}$$

Design of the control system with respect to CLF (B.1) ensures elimination of joint angle tracking error e_1 according to (B.3), elimination of endpoint vibration e_2 according to (B.5), mitigation of distributed displacements and higher-order derivatives with respect to (B.4) and boundary conditions (11) and (12), and robustness despite the presence of parametric uncertainty based on (B.6).

To ensure that a Lyapunov function can be assigned based on CLF (B.1), the conditions through which $V > 0$ holds are demonstrated. This is trivially true if $V_b > 0$. Hence, the conditions for satisfying the latter and weaker conditions are investigated.

Based on the Cauchy–Schwartz and Nash inequalities (as expressed in Remark 4), it holds that:

$$\left|\int_0^l \xi\omega_t(\xi)\omega_\xi(\xi)\,d\xi\right| < l\int_0^l \omega_t^2(\xi)\,d\xi + l\int_0^l \omega_\xi^2(\xi)\,d\xi < l\int_0^l \omega_t^2(\xi)\,d\xi + l^3\int_0^l \omega_{\xi\xi}^2(\xi)\,d\xi. \tag{B.7}$$

Substituting (B.7) in (B.4) results in:

$$V_b > \frac{1}{2}(\alpha-\beta l)\int_0^l \omega_t^2(\xi)\,d\xi + \frac{1}{2}\left(\alpha\frac{\hat{E}\hat{I}}{\hat{\rho}\hat{A}} - \beta l^3\right)\int_0^l \omega_{\xi\xi}^2(\xi)\,d\xi. \tag{B.8}$$

Hence, the condition for positivity of V is obtained as follows:

$$\alpha > \max\left(\beta l, \beta\frac{\rho A}{EI}l^3\right). \tag{B.9}$$

Subsequently, we determine the conditions for the decay of V_t and V_f on their own. Then, the combined information is used to obtain the control law in combination with the conditions for decay of V_s.

Initially, the time derivate of V_t is analyzed based on (B.3)

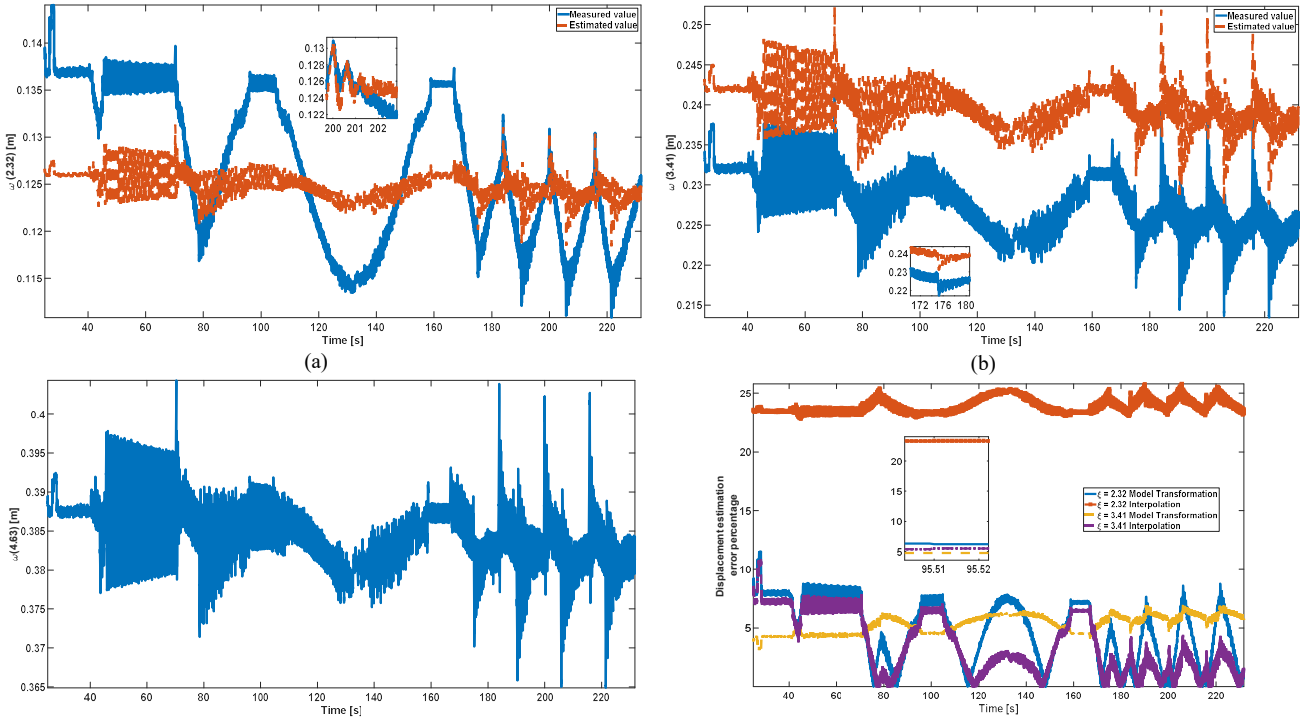

Fig. 11. Displacement values for selected points: (a) $\xi = 2.32\ [m]$; (b) $\xi = 3.41\ [m]$; (c) $\xi = 4.63\ [m]$; (d) Displacement estimation error percentage.

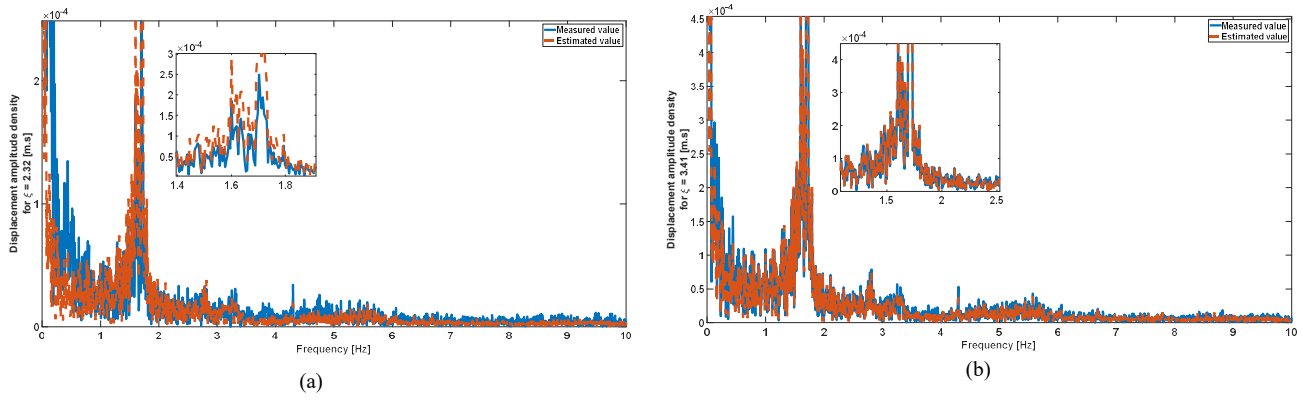

Fig. 12. Density analysis per frequency for displacement amplitude and its estimation: (a) $\xi = 2.32\ [m]$; (b) $\xi = 3.41\ [m]$.

and (27).

$$\dot{V}_t = e_1\dot{e}_1 = e_1\nu_1 + e_1\gamma_{11}\tau + e_1\gamma_{12}u. \tag{B.10}$$

It is assigned that:

$$e_1\nu_1 + e_1\gamma_{11}\tau + e_1\gamma_{12}u = -\delta_1^2, \tag{B.11}$$

where $\delta_1 > 0$ is a control parameter.

Next, the time derivative of V_f is investigated based on (9), (28), and (A.10), using successive integration-by-parts.

$$\begin{aligned}\dot{V}_f = \dot{V}_b + \dot{V}_e &= e_2\nu_2 + e_2\gamma_{21}\tau + e_2\gamma_{22}u \\ &+ \alpha\int_0^l \omega_t(\xi)\omega_{tt}(\xi)d\xi \\ &+ \alpha\int_0^l \frac{EI}{\rho A}\omega_{\xi\xi}(\xi)\omega_{t\xi\xi}(\xi)\,d\xi \\ &+ \beta\int_0^l \xi\omega_{tt}(\xi)\omega(\xi)\,d\xi \\ &+ \beta\int_0^l \xi\omega_t\omega_{\xi t}\,d\xi + e_2\dot{e}_2 \\ &= e_2\nu_2 + e_2\gamma_{21}\tau + e_2\gamma_{22}u \\ &+ \alpha\int_0^l \left\{\left[\omega(\xi)\dot{\theta}^2 - \frac{EI}{\rho A}\omega_{\xi\xi\xi\xi}(\xi)\right.\right. \\ &\left.\left. - \xi\ddot{\theta}\right]\omega_t(\xi)\right\}d\xi \\ &+ \alpha\frac{EI}{\rho A}\int_0^l \omega_{\xi\xi\xi\xi}(\xi)\omega_t(\xi)\,d\xi \\ &- \alpha\frac{EI}{\rho A}\omega_t(l)\omega_{\xi\xi\xi}(l) \\ &+ \beta\int_0^l \left\{\left[\xi\omega(\xi)\dot{\theta}^2 - \frac{EI}{\rho A}\xi\omega_{\xi\xi\xi\xi}(\xi)\right.\right. \\ &\left.\left. - \xi^2\ddot{\theta}\right]\omega(\xi)\right\} + \frac{1}{2}\beta l\omega_t^2(l) \\ &- \frac{1}{2}\beta\int_0^l \omega_t^2(\xi)\,d\xi\end{aligned} \tag{B.12}$$

$\dot{V}_f$ is alternatively expressed as:

$$\dot{V}_f = m_f\ddot{\theta} + h_f + e_2\nu_2 + e_2\gamma_{21}u_1 + e_2\gamma_{22}u_2, \tag{B.13}$$

$$m_f = -\alpha\int_0^l \xi\omega_t(\xi)d\xi - \beta\int_0^l \xi^2\omega(\xi)d\xi, \tag{B.14}$$

$$\begin{aligned}h_f = {} & \alpha\dot{\theta}^2\int_0^l \omega_t(\xi)\omega(\xi)\,d\xi - \alpha\tfrac{EI}{\rho A}\omega_t(l)\omega_{\xi\xi\xi}(l) + \\ & \beta\dot{\theta}^2\int_0^l \xi\omega^2(\xi)\,d\xi - \beta\tfrac{EI}{\rho A}\int_0^l \omega(\xi)\,\omega_{\xi\xi\xi\xi}(\xi) - \\ & \tfrac{1}{2}\beta\int_0^l \omega_t^2(\xi)d\xi + \tfrac{1}{2}\beta l\,\omega_t^2(l).\end{aligned} \tag{B.15}$$

From (15), it holds that:

$$\ddot{\underline{q}} = \underline{\boldsymbol{\nu}}_0 + \underline{\boldsymbol{\gamma}}_0\underline{\boldsymbol{u}}, \tag{B.16}$$

$$\underline{\boldsymbol{\nu}}_0 = -\underline{\boldsymbol{M}}^{-1}\underline{\boldsymbol{h}}, \tag{B.17}$$

$$\underline{\boldsymbol{\gamma}}_0 = \underline{\boldsymbol{M}}^{-1}\underline{\boldsymbol{B}}. \tag{B.18}$$

Hence, $\ddot{\theta}$ is expressible as follows:

$$\ddot{\theta} = \nu_{0_1} + \gamma_{0_{11}}\tau + \gamma_{0_{12}}u. \tag{B.19}$$

Subsequently, the simplified expression of $\dot{V}_f$ is obtained by substituting (B.19) in (B.12). Furthermore, it is set that $\dot{V}_f = -\delta_2^2$, where $\delta_2 > 0$ is a control parameter.

$$\begin{aligned}\dot{V}_f = {} & \left(m_f\gamma_{0_{11}} + e_2\gamma_{21}\right)\tau + \left(m_f\gamma_{0_{12}} + e_2\gamma_{22}\right)u + m_f\nu_{0_1} \\ & + e_2\nu_2 + h_f = -\delta_2^2\end{aligned} \tag{B.20}$$

To obtain the input resulting in the decay of V_t and V_f, (B.10) and (B.20) are combined in matrix form as follows:

$$\boldsymbol{\mathcal{M}}\underline{\boldsymbol{u}} = \boldsymbol{\hbar} - \boldsymbol{\delta}, \tag{B.21}$$

$$\boldsymbol{\mathcal{M}} = \begin{bmatrix} e_1\gamma_{11}, & e_1\gamma_{12} \\ m_f\gamma_{0_{11}} + e_2\gamma_{21}, & m_f\gamma_{0_{12}} + e_2\gamma_{22}\end{bmatrix}, \tag{B.22}$$

$$\boldsymbol{\hbar} = \begin{bmatrix} -e_1\nu_1 \\ -e_2\nu_2 - m_f\nu_{0_1} - h_f\end{bmatrix}. \tag{B.23}$$

$$\boldsymbol{\delta} = \begin{bmatrix}\delta_1^2 \\ \delta_2^2\end{bmatrix}. \tag{B.24}$$

(B.21) is instantly solvable for $\underline{\boldsymbol{u}}$, leading to:

$$\underline{\boldsymbol{u}} = \boldsymbol{\mathcal{M}}^{-1}\boldsymbol{\hbar}, \tag{B.25}$$

which results in $\dot{V}_t + \dot{V}_f = tr(\boldsymbol{\mathcal{M}}\underline{\boldsymbol{u}} - \boldsymbol{\hbar}) = -\delta_1^2 - \delta_2^2 < 0$. $tr(.)$ indicates the trace of $(.)$. The boundedness of the controller in the presence of model uncertainty is investigated as (B.26). In this case, the estimated control input $\underline{\widehat{\boldsymbol{u}}}$ expressed in (34) is exerted to the system.

To address parametric uncertainty, the time derivative of V_s is investigated as follows:

$$\dot{V}_s = \underline{\tilde{\boldsymbol{s}}}^T\underline{\dot{\tilde{\boldsymbol{s}}}} = \left(\underline{\dot{\boldsymbol{s}}} - \underline{\dot{\hat{\boldsymbol{s}}}}\right)^T\left(\underline{\boldsymbol{s}} - \underline{\hat{\boldsymbol{s}}}\right) = -\underline{\dot{\hat{\boldsymbol{s}}}}^T\left(\underline{\boldsymbol{s}} - \underline{\hat{\boldsymbol{s}}}\right). \tag{B.26}$$

Then, from (B.1), (B.10), (B.12), (B.13), (B.20), and (B.26) and considering terms dependent on uncertain parameter $s_2 = \frac{EI}{\rho A}$ in (B.12), it follows that:

$$\begin{aligned}\dot{V} = \tilde{s}_2\left\{\int_0^l\left[-\omega_{\xi\xi\xi\xi}(\xi)\omega_t(\xi) + \right.\right. \\ \left.\alpha\int_0^l \omega_{\xi\xi\xi\xi}(\xi)\omega_t(\xi) - \beta - \xi\omega_{\xi\xi\xi\xi}(\xi)\right]d\xi - \\ \left.\alpha\omega_t(l)\omega_{\xi\xi\xi}(l)\right\} - \underline{\dot{\hat{\boldsymbol{s}}}}^T\left(\underline{\boldsymbol{s}} - \underline{\hat{\boldsymbol{s}}}\right) + tr\left(\boldsymbol{\mathcal{M}}\underline{\boldsymbol{u}} - \boldsymbol{\hbar}\right).\end{aligned} \tag{B.27}$$

Considering the uncertainty space $\mathcal{Q}$ from Assumption 2 and system input (34), $tr\left(\boldsymbol{\mathcal{M}}\underline{\boldsymbol{u}} - \boldsymbol{\hbar}\right)$ is bounded as:

$$\begin{aligned}tr\left(\boldsymbol{\mathcal{M}}\underline{\boldsymbol{u}} - \boldsymbol{\hbar}\right) &= tr\left(\widehat{\boldsymbol{\mathcal{M}}}\underline{\widehat{\boldsymbol{u}}} - \widehat{\boldsymbol{\hbar}}\right) + e_Q \\ &\leq -\delta_1^2 - \delta^2 + e_Q,\end{aligned} \tag{B.28}$$

$$\epsilon_Q = tr\left(\widetilde{\boldsymbol{\mathcal{M}}}\underline{\widehat{\boldsymbol{u}}} - \widetilde{\boldsymbol{\hbar}}\right), \tag{B.29}$$

where $\widetilde{\boldsymbol{\mathcal{M}}} = \boldsymbol{\mathcal{M}} - \widehat{\boldsymbol{\mathcal{M}}}$ and $\widetilde{\boldsymbol{\hbar}} = \boldsymbol{\hbar} - \widehat{\boldsymbol{\hbar}}$. From Assumption 2, it follows that ϵ_Q is expressible as a function of $\underline{\tilde{\boldsymbol{s}}}$, with its upper bound expressible as $\underline{\boldsymbol{\lambda}}_Q^T\,\underline{\tilde{\boldsymbol{s}}}$, where $\underline{\boldsymbol{\lambda}}_Q \epsilon \mathbb{R}^4$. Substituting (B.28) in (B.27), it follows that:

$$\dot{V} \leq \lambda_s\tilde{s}_2 - \underline{\dot{\hat{\boldsymbol{s}}}}^T\underline{\tilde{\boldsymbol{s}}} - \delta_1^2 - \delta_2^2 + \underline{\boldsymbol{\lambda}}_Q^T\,\underline{\tilde{\boldsymbol{s}}}, \tag{B.30}$$

$$\begin{aligned}\lambda_s = \int_0^l\left[-\omega_{\xi\xi\xi\xi}(\xi)\omega_t(\xi) + \right. \\ \left.\alpha\int_0^l \omega_{\xi\xi\xi\xi}(\xi)\omega_t(\xi) - \beta - \xi\omega_{\xi\xi\xi\xi}(\xi)\right]d\xi - \\ \alpha\omega_t(l)\omega_{\xi\xi\xi}(l).\end{aligned} \tag{B.31}$$

The term $\lambda_s\tilde{s}_2 - \underline{\dot{\hat{\boldsymbol{s}}}}^T\underline{\tilde{\boldsymbol{s}}}$ is rewritten in vector form as follows:

$$\lambda_s\tilde{s}_2 - \underline{\dot{\hat{\boldsymbol{s}}}}^T\underline{\tilde{\boldsymbol{s}}} + \underline{\boldsymbol{\lambda}}_Q^T\,\underline{\tilde{\boldsymbol{s}}} = \left(\boldsymbol{\Lambda}_s + \underline{\boldsymbol{\lambda}}_Q - \underline{\dot{\hat{\boldsymbol{s}}}}\right)^T\underline{\tilde{\boldsymbol{s}}}, \tag{B.32}$$

$$\boldsymbol{\Lambda}_s = [0, \quad \lambda_s, \quad 0, \quad 0]^T. \tag{B.33}$$

Substituting (B.32) and parameter update rule (35) in (B.30) and then using Lemma 1 leads to:

$$\begin{aligned}\dot{V} \leq \left[\boldsymbol{\Lambda}_s + \underline{\boldsymbol{\lambda}}_Q - \mathcal{P}\left(\underline{\boldsymbol{s}}, \underline{\boldsymbol{s}}_{l'}, \underline{\boldsymbol{s}}_h, \underline{\boldsymbol{\lambda}}_Q + \underline{\boldsymbol{\Lambda}}_s\right)\right]^T - \delta_1^2 - \\ \delta^2 \leq -\delta_1^2 - \delta_2^2.\end{aligned} \tag{B.34}$$

Hence, the closed-loop system is asymptotically stable, and e_1, e_2, $\omega(\xi)$, and $\underline{\tilde{\boldsymbol{s}}}^T\underline{\tilde{\boldsymbol{s}}}$ converge to zero with $t \to \infty$, which completes the proof.

Appendix C. Proof of Theorem 2

To obtain the transformed model, (37) and (52) are substituted in the flexible system model (8), (9), (11), (12), and (30). In addition, the following expressions hold:

$$\frac{\partial^n z}{\partial \xi^n} = \frac{\partial^n \omega}{\partial \xi^n} + \frac{\partial^n \gamma}{\partial \xi^n} f_b^*, \tag{C.1}$$

$$\frac{\partial^n z}{\partial t^n} = \frac{\partial^n \omega}{\partial t^n} + \gamma \frac{\partial^n f_b^*}{\partial t^n}, \tag{C.2}$$

$$z(l) = \omega(l). \tag{C.3}$$

An expression of the transformed model is then obtained as follows:

$$\begin{aligned}&[I_m + Ml^2 + Mz^2(l)]\ddot{\theta} + Ml\gamma(l)f_{btt}^* - Mlz_{tt}(l) + \\ &2Mz(l)\gamma(l)f_{bt}^* - 2Mz(l)z_t(l) + \\ &\rho A\int_0^l\{2z(\xi)z_t(\xi)\dot{\theta} - 2z(\xi)\gamma(\xi)f_{bt}^*\dot{\theta} - \\ &2v(\xi)z_t(\xi)\dot{\theta} + 2v^2(\xi)\dot{\theta} + [z^2(\xi) - 2z(\xi)v(\xi) + \\ &v^2(\xi)]\ddot{\theta} + \xi z_{tt}(\xi) - \xi\gamma(\xi)f_{btt}^*\}d\xi + \\ &\frac{1}{2}mgl\cos\theta + Mgl\cos\theta + Mgz(l)\sin\theta = \tau + ul,\end{aligned} \tag{C.4}$$

$$\begin{aligned}&z_{tt}(\xi) - \gamma(\xi)f_{btt}^* - z(\xi)\dot{\theta}^2 + v(\xi)\dot{\theta}^2 + \xi\ddot{\theta} + \\ &\frac{EI}{\rho A}z_{\xi\xi\xi\xi}(\xi) - \frac{EI}{\rho A}\gamma_{\xi\xi\xi\xi}(\xi)f_b^* = 0,\end{aligned} \tag{C.5}$$

along with boundary conditions (36)–(38). Substituting $f_{bt}^* = k\ddot{u} - \kappa g\dot{\theta}\sin\theta$ and $f_{btt}^* = k\ddot{u} - \kappa g\ddot{\theta}\sin\theta - \kappa g\dot{\theta}^2\cos\theta$ and noting that $\gamma(l) = 0$, (C.4) and (C.5) are further simplified as follows:

$$\begin{aligned}&[I_m + Ml^2 + M\omega^2(l)]\ddot{\theta} - Mlz_{tt}(l) - \\ &2Mz(l)z_t(l) + \rho A\int_0^l\{2z(\xi)z_t(\xi)\dot{\theta} - \\ &2z(\xi)\gamma(\xi)k\ddot{u}\dot{\theta} + 2z(\xi)\gamma(\xi)\kappa g\dot{\theta}^2\sin\theta - \\ &2v(\xi)z_t(\xi)\dot{\theta} + 2v^2(\xi)\dot{\theta} + [z^2(\xi) - 2z(\xi)v(\xi) + \\ &v^2(\xi)]\ddot{\theta} + \xi z_{tt}(\xi) - \xi\gamma(\xi)k\ddot{u} + \xi\gamma(\xi)\kappa g\ddot{\theta}\sin\theta + \\ &\xi\gamma(\xi)\kappa g\cos\theta\}d\xi + \frac{1}{2}mgl\cos\theta + Mgl\cos\theta + \\ &Mgz(l)\sin\theta = \tau + ul,\end{aligned} \tag{C.6}$$

$$\begin{aligned}&z_{tt}(\xi) - \gamma(\xi)k\ddot{u} + \gamma(\xi)\kappa g\ddot{\theta}\sin\theta + \\ &\gamma(\xi)\kappa g\dot{\theta}^2\cos\theta - z(\xi)\dot{\theta}^2 + v(\xi)\dot{\theta}^2 + \xi\ddot{\theta} + \\ &\frac{1}{\kappa}z_{\xi\xi\xi\xi}(\xi) - \gamma_{\xi\xi\xi\xi}(\xi)u + \gamma_{\xi\xi\xi\xi}(\xi)g\cos\theta = 0.\end{aligned} \tag{C.7}$$

The homogenized model may be further simplified using the expression $\int_0^l \xi z_{tt}d\xi$ as well as calculating the integration terms of the known function $v(\xi)$, which based on (44) is expressible as (B.8).

$$v(\xi) = \gamma(\xi)\kappa u - \gamma(\xi)\kappa g\cos\theta \tag{C.8}$$

By substituting (B.8) in (B.6) and noting $\gamma_{\xi\xi\xi\xi}(\xi) = -\gamma_1 e^{-p}$, $\int_0^l \xi z_{tt}d\xi$ is calculated as follows:

$$\begin{aligned}\int_0^l \xi z_{tt}d\xi &= \int_0^l \xi\Big[\gamma(\xi)k\ddot{u} - \gamma(\xi)\kappa g\ddot{\theta}\sin\theta - \\ &\gamma(\xi)\kappa g\dot{\theta}^2\cos\theta + z(\xi)\dot{\theta}^2 - v(\xi)\dot{\theta}^2 - \xi\ddot{\theta} - \\ &\frac{1}{\kappa}z_{\xi\xi\xi\xi}(\xi) + \gamma_{\xi\xi\xi\xi}(\xi)u - \gamma_{\xi\xi\xi\xi}(\xi)g\cos\theta\Big]d\xi = \\ &k\ddot{u}\int_0^l \xi\gamma(\xi)\,d\xi - \kappa g\ddot{\theta}\sin\theta\int_0^l \xi\gamma(\xi)\,d\xi - \\ &\kappa g\dot{\theta}^2\cos\theta\int_0^l \xi\gamma(\xi)\,d\xi + \dot{\theta}^2\int_0^l \xi z(\xi)\,d\xi - \\ &\kappa u\dot{\theta}^2\int_0^l \xi\gamma(\xi)d\xi + \kappa g\cos\theta\,\dot{\theta}^2\int_0^l \xi\gamma(\xi)d\xi - \\ &\ddot{\theta}\int_0^l \xi^2\,d\xi - \frac{1}{\kappa}\int_0^l \xi z_{\xi\xi\xi\xi}(\xi)d\xi + (u - \\ &g\cos\theta)\int_0^l \xi\gamma_{\xi\xi\xi\xi}(\xi)\,d\xi.\end{aligned} \tag{C.9}$$

Based on the definition of $\gamma(\xi)$ in (53), the integral terms $\int_0^l \xi\gamma(\xi)\,d\xi$ and $\int_0^l \xi\gamma_{\xi\xi\xi\xi}(\xi)\,d\xi$ attain constant values.

$$\begin{aligned}p_1 = \int_0^l \xi\gamma(\xi)\,d\xi &= \int_0^l \Big[-\frac{\gamma_1}{p^4}\xi e^{-p\xi} + \frac{1}{6p}\xi^4 + \gamma_2\xi^3 \\ &- \frac{\gamma_1}{p^3}\xi^2 + \frac{\gamma_1}{p^4}\xi\Big]d\xi \\ &= \Big(\frac{l}{p^5} + \frac{1}{p^6}\Big)\gamma_1 e^{-pl} - \frac{\gamma_1}{p^6} + \frac{l^5}{30p} \\ &+ \gamma_2\frac{l^4}{4} - \frac{\gamma_1 l^3}{3p^3} + \frac{\gamma_1 l^2}{2p^4}\end{aligned} \tag{C.10}$$

$$\begin{aligned}p_2 = \int_0^l \xi\gamma_{\xi\xi\xi\xi\xi}(\xi)\,d\xi &= -\gamma_1\int_0^l \xi\, e^{-p\xi}d\xi \\ &= \frac{\gamma_1 l}{p}e^{-pl} + \frac{\gamma_1}{p^2}e^{-pl} - \frac{\gamma_1}{p^2}\end{aligned} \tag{C.11}$$

Substituting (C.10) and (C.11) in (C.9) results in the simplified expression (C.12), as follows:

$$\begin{aligned}&\int_0^l \xi z_{tt}d\xi = p_1 k\ddot{u} - p_1\kappa g\ddot{\theta}\sin\theta + \dot{\theta}^2\int_0^l \xi z(\xi)\,d\xi - \\ &\kappa u\dot{\theta}^2 p_2 - \frac{l^3}{3}\ddot{\theta} - \frac{1}{\kappa}\int_0^l \xi z_{\xi\xi\xi\xi}(\xi)d\xi + p_2(u - g\cos\theta).\end{aligned} \tag{C.12}$$

Finally, substituting (C.12) in (C.6), the simplified homogenized model is obtained as in (54)–(58) with the homogenized boundary conditions (38)–(40). This completes the proof.

REFERENCES

[1] W. Chen, "Dynamic modeling of multi-link flexible robotic manipulators," *Comput Struct*, vol. 79, no. 2, pp. 183–195, Jan. 2001, doi: 10.1016/S0045-7949(00)00129-2.

[2] X. Zhang, W. Xu, S. S. Nair, and V. S. Chellaboina, "PDE Modeling and Control of a Flexible Two-Link Manipulator," *IEEE Trans Control Syst Technol*, vol. 13, no. 2, pp. 301–312, 2005, doi: 10.1109/TCST.2004.842446.

[3] S. S. Rao, *Vibration of Continuous Systems (2007)*. Hoboken, New Jersey: John Wileys, 2007.

[4] M. R. Homaeinezhad, F. FotoohiNia, and S. Yaqubi, "Active predictive vibration suppression algorithm for structural stability and tracking control of nonlinear multivariable continuum-mechanics mobile systems," *Optim Control Appl Methods*, 2020, doi: 10.1002/oca.2687.

[5] P. Mäkinen and J. Mattila, "Finite Element-Based Control of a Single-Link Flexible Hydraulic Manipulator," in *ASME/BATH 2017 Symposium on Fluid Power and Motion Control*, American Society of Mechanical Engineers, Oct. 2017, pp. 248–253. doi: 10.1115/FPMC2017-4264.

[6] P. Staufer and H. Gattringer, "State estimation on flexible robots using accelerometers and angular rate sensors," *Mechatronics*, vol. 22, no. 8, pp. 1043–1049, Dec. 2012, doi: 10.1016/j.mechatronics.2012.08.009.

[7] Z. Han, Z. Liu, W. Kang, and W. He, "Boundary Feedback Control of a Nonhomogeneous Wind Turbine Tower With Exogenous Disturbances," *IEEE Trans Automat Contr*, vol. 67, no. 4, pp. 1952–1959, Apr. 2022, doi: 10.1109/TAC.2021.3071021.

[8] K. Mathiyalagan, A. Shree Nidhi, and T. Renugadevi, "Boundary stabilization and state estimation of ODE-transport PDE with in-domain coupling," *J Franklin Inst*, vol. 359, no. 2, pp. 1605–1625, Jan. 2022, doi: 10.1016/j.jfranklin.2021.11.028.

[9] H. Yang, J. Liu, and X. Lan, "Observer design for a flexible-link manipulator with PDE model," *J Sound Vib*, vol. 341, pp. 237–245, Apr. 2015, doi: 10.1016/j.jsv.2014.12.033.

[10] J. Wang, J. Liu, B. Ji, Y. He, S. Xia, and Y. Zhou, "Vibration suppression and boundary control for nonlinear flexible rotating manipulator in three-dimensional space subject to

output restrictions," *Commun Nonlinear Sci Numer Simul*, vol. 120, Jun. 2023, doi: 10.1016/j.cnsns.2023.107151.

[11] X.-Y. Zhang, Y.-X. Li, and C. K. Ahn, "Prescribed finite-time boundary control of constrained flexible satellite systems with translational motion modeling," *Aerosp Sci Technol*, p. 108470, Sep. 2023, doi: 10.1016/j.ast.2023.108470.

[12] F. Cao and J. Liu, "An adaptive iterative learning algorithm for boundary control of a coupled ODE–PDE two-link rigid–flexible manipulator," *J Franklin Inst*, vol. 354, no. 1, pp. 277–297, 2017, doi: 10.1016/j.jfranklin.2016.10.013.

[13] W. He, X. He, M. Zou, and H. Li, "PDE Model-Based Boundary Control Design for a Flexible Robotic Manipulator with Input Backlash *IEEE Trans Control Syst Technol*, vol. 27, no. 2, pp. 790–797, 2019, doi: 10.1109/TCST.2017.2780055.

[14] N. Ji and J. Liu, "Vibration Control for a Three-Dimensional Variable Length Flexible String With Time-Varying Actuator Faults and Unknown Control Directions," *IEEE Trans. Autom. Sci. Eng*, 2022, doi: 10.1109/TASE.2022.3200711.

[15] Y. Cheng, Y. Li, Y. Wu, and K.-S. Hong, "Anti-disturbance control for a nonlinear flexible beam with velocity disturbance at the boundary," *Automatica*, vol. 152, p. 110978, Jun. 2023, doi: 10.1016/j.automatica.2023.110978.

[16] L. Li and J. Liu, "Nussbaum function-based adaptive boundary control for flexible manipulator with unknown control directions and nonlinear time-varying actuator faults," *Int. J. Robust Nonlinear Control*, 2023, doi: 10.1002/rnc.6723.

[17] S. Zhang, Y. Wu, X. He, and Z. Liu, "Cooperative Fault-Tolerant Control for a Mobile Dual Flexible Manipulator With Output Constraints," *IEEE Trans. Autom. Sci. Eng*, vol. 19, no. 4, pp. 2689–2698, Oct. 2022, doi: 10.1109/TASE.2021.3102588.

[18] S. K. Pradhan and B. Subudhi, "Real-time adaptive control of a flexible manipulator using reinforcement learning," *IEEE Trans. Autom. Sci. Eng*, vol. 9, no. 2, pp. 237–249, Apr. 2012, doi: 10.1109/TASE.2012.2189004.

[19] P. K. Kythe, M. R. Schäferkotter, and P. Puri, *Partial Differential Equations and Mathematica*. United Kingdom, London: Chapman and Hall/CRC, 2018. doi: 10.1201/9781315273105.

[20] F. Cao and J. Liu, "Boundary control for a constrained two-link rigid–flexible manipulator with prescribed performance," *Int J Control*, vol. 91, no. 5, pp. 1091–1103, 2018, doi: 10.1080/00207179.2017.1305513.

[21] N. A. Apetre, J. G. Michopoulos, J. C. Steuben, A. J. Birnbaum, and A. P. Iliopoulos, "Analytical thermoelastic solutions for additive manufacturing processes," *Addit Manuf*, vol. 56, Aug. 2022, doi: 10.1016/j.addma.2022.102892.

[22] W. He and S. S. Ge, "Robust adaptive boundary control of a vibrating string under unknown time-varying disturbance," *IEEE Trans Control Syst Technol*, vol. 20, no. 1, pp. 48–58, Jan. 2012, doi: 10.1109/TCST.2010.2099230.

[23] F. Guo, Y. Liu, Y. Wu, and F. Luo, "Observer-based backstepping boundary control for a flexible riser system," *Mech Syst Signal Process*, vol. 111, pp. 314–330, 2018, doi: 10.1016/j.ymssp.2018.03.058.

[24] H. K. Rad, H. Salarieh, A. Alasty, and R. Vatankhah, "Boundary control of flexible satellite vibration in planar motion," *J Sound Vib*, vol. 432, pp. 549–568, 2018, doi: 10.1016/j.jsv.2018.06.052.

[25] M. M. Ataei, H. Salarieh, H. N. Pishkenari, and H. Jalili, "Boundary control design for vibration suppression and attitude control of flexible satellites with multi-section appendages," *Acta Astronaut*, vol. 173, no. March, pp. 22–30, 2020, doi: 10.1016/j.actaastro.2020.04.001.

[26] W.-H. Zhu, *Virtual Decomposition Control*, vol. 60. in Springer Tracts in Advanced Robotics, vol. 60. Germany, Berlin, Heidelberg: Springer Berlin Heidelberg, 2010. doi: 10.1007/978-3-642-10724-5.

[27] Y. Liu, X. Chen, Y. Wu, H. Cai, and H. Yokoi, "Adaptive Neural Network Control of a Flexible Spacecraft Subject to Input Nonlinearity and Asymmetric Output Constraint," *IEEE Trans Neural Netw Learn Syst*, vol. 33, no. 11, pp. 6226–6234, Nov. 2022, doi: 10.1109/TNNLS.2021.3072907.

[28] B. Zhan, M. Jin, and J. Liu, "Extended-state-observer-based adaptive control of flexible-joint space manipulators with system uncertainties," *Advances in Space Research*, vol. 69, no. 8, pp. 3088–3102, 2022, doi: 10.1016/j.asr.2022.01.016.

[29] L. Zhang and J. Liu, "Observer-based partial differential equation boundary control for a flexible two-link manipulator in task space," *IET Control. Theory Appl.*, vol. 6, no. 13, pp. 2120–2133, Sep. 2012, doi: 10.1049/iet-cta.2011.0545.

[30] Z. Zhao, Z. Liu, W. He, K. S. Hong, and H. X. Li, "Boundary adaptive fault-tolerant control for a flexible Timoshenko arm with backlash-like hysteresis," *Automatica*, vol. 130, p. 109690, 2021, doi: 10.1016/j.automatica.2021.109690.

[31] W. He, S. S. Ge, B. V. E. How, Y. S. Choo, and K. S. Hong, "Robust adaptive boundary control of a flexible marine riser with vessel dynamics," *Automatica*, vol. 47, no. 4, pp. 722–732, 2011, doi: 10.1016/j.automatica.2011.01.064.

[32] T. Jiang, J. Liu, and W. He, "Boundary control for a flexible manipulator based on infinite dimensional disturbance observer," *J Sound Vib*, vol. 348, pp. 1–14, 2015, doi: .

[33] Y. Liu, W. Zhan, M. Xing, Y. Wu, R. Xu, and X. Wu, "Boundary Control of a Rotating and Length-Varying Flexible Robotic Manipulator System," *IEEE Trans Syst Man Cybern Syst*, vol. 52, no. 1, pp. 377–386, Jan. 2022, doi: 10.1109/TSMC.2020.2999485.

[34] F. Guo, Y. Liu, Y. Wu, and F. Luo, "Observer-based backstepping boundary control for a flexible riser system," *Mech Syst Signal Process*, vol. 111, pp. 314–330, 2018, doi: 10.1016/j.ymssp.2018.03.058.

[35] J. Nash, "Continuity of Solutions of Parabolic and Elliptic Equations," *American Journal of Mathematics*, vol. 80, no. 4, p. 931, Oct. 1958, doi: 10.2307/2372841.

[36] C. D. Rahn, *Mechatronic Control of Distributed Noise and Vibration*. 2001. doi: 10.1007/978-3-662-04641-8.

[37] Zheng-Hua Luo, "Direct strain feedback control of flexible robot arms: new theoretical and experimental results," *IEEE Trans Automat Contr*, vol. 38, no. 11, pp. 1610–1622, 1993, doi: 10.1109/9.262031.

[38] Y. Liu, Y. Mei, H. Cai, C. He, T. Liu, and G. Hu, "Asymmetric Input-Output Constraint Control of a Flexible Variable-Length Rotary Crane Arm," *IEEE Trans Cybern*, vol. 52, no. 10, pp. 10582–10591, Oct. 2022, doi: 10.1109/TCYB.2021.3055151.

S. Yaqubi received his Ph.D. in mechanical engineering from K. N. Toosi University of Technology (Iran). He is currently with Tampere University (Finland) as a postdoctoral researcher in Department of Automation Technology and Mechanical Engineering. His research interests include control systems theory, nonlinear dynamics, intelligent systems, and optimization.

S. Mohammad Tahamipour-Z. received his B.Sc. and M.Sc. degrees in Electrical Engineering-control from Iran University of Science and Technology (IUST), Tehran, and Ferdowsi University of Mashhad (FUM), Mashhad, Iran, in 2016 and 2019, respectively. He is currently a Ph.D. student in Automation Technology and Mechanical Engineering at Tampere University (TAU), Tampere, Finland. His research interests include artificial intelligence (AI) algorithms, model predictive control (MPC), and nonlinear model-based control applications in robotics.

Jouni Mattila received the M.Sc. (Eng.) and Dr.Tech. degrees from Tampere University of Technology (TUT), Tampere, Finland, in 1995 and 2000, respectively. He is currently a Professor of machine automation with the unit of Automation Technology and Mechanical Engineering, Tampere University. His current research interests include machine automation, nonlinear model-based control of robotic manipulators, and energy-efficient control of heavy-duty mobile manipulators.